



## Review

# Non-silica periodic mesostructured materials: recent progress

Abdelhamid Sayari \*, Ping Liu

*Department of Chemical Engineering and CERPIC, Université Laval, Ste-Foy, Que., Canada, G1K 7P4*

Received 31 March 1997; accepted 8 July 1997

---

**Keywords:** Mesoporous materials; Non-silica mesoporous materials; Molecular sieves; Templating mechanisms; Supramolecular templates; Surfactant MCM-41; M41S materials

---

## 1. Summary

The discovery of M41S periodic mesoporous silicates in 1991–1992 based on the use of surfactant supramolecular templates had an immediate strong impact on the area of mesostructured inorganic materials. A variety of related synthesis strategies have been developed while a great diversity of materials in terms of both composition and structure has been achieved. This review deals with non-silica mesostructured materials. Supramolecular templating techniques based on electrostatic interactions (ionic bonding), van der Waals interactions (hydrogen bonding) and direct covalent bonding between organic and inorganic species are presented, discussed and evaluated. Important issues, particularly regarding thermal stability of the materials, have been identified for future research.

## 2. Introduction

The design and synthesis of organic, inorganic and polymeric materials with controlled pore struc-

ture are important academic and industrial issues [1–7]. In many applications, the precise control of pore dimensions, sometimes to a fraction of an ångstrom, is the dividing line between success and failure [8]. Zeolites, molecular sieves, pillared clays, porous carbons and polymers are common examples of such materials. Ideally, a porous material would have the following properties: (i) a narrow pore size distribution which is a critical requirement for such applications as shape selective catalysis or the separation of gas and liquid mixtures based on molecular sizes; (ii) a readily tunable pore size in a wide range which affords added flexibility in matching the pore size with application requirements. This is in addition to more standard properties such as high chemical, thermal, hydrothermal and mechanical stability, appropriate particle size, high surface area and pore volume, etc.

Zeolites and other zeolite-like molecular sieves (zeotypes) often fulfill the above requirements. Hence, they find important applications in adsorption and gas separation [9,10], ion-exchange [11] and catalysis [12,13]. Other potential applications include intrazeolite fabrication technology, such as the encapsulation of semiconductor clusters, advanced materials with unique electronic and

\* Corresponding author. Tel: +1 418 6563563;  
Fax: +1 418 6565993; e-mail: sayari@gch.ulaval.ca

optical properties, enzyme mimicking organometallic complexes, etc. [14–18].

Microporous zeotypes include four subgroups: small, medium, large and extra-large pore molecular sieves, with pore openings comprised of 8, 10, 12 and more than 12 tetrahedral (T) atoms, respectively. Until recently, the only known extra-large pore zeotypes were metallophosphates, including AlPO<sub>4</sub>-8, ULM-5, VPI-5, Cloverite and JDF-20 with 14-, 16-, 18-, 20- and 20-membered rings, respectively [19–23]. The first extra-large pore aluminosilicate, UTD-1, with 14-membered rings has been discovered recently [24]. Several excellent reviews dealing with the design, synthesis, characterization and current as well as potential applications of microporous zeotypes are available [12–15,25–29].

While zeotypes are being used in many commercially important applications where the occurrence of a well-defined micropore system is required or desirable, there was a persistent demand for crystalline mesoporous materials because of their potential applications as (i) catalysts in processes such as heavy oil hydrocracking and catalytic conversion of large molecules, (ii) separation media, or (iii) hosts for bulky molecules for advanced materials applications. Until very recently, most available mesoporous materials were amorphous and often with broad pore size distributions.

In 1992, researchers at Mobil R&D Corporation extended the templating strategy commonly used for zeolite synthesis to the preparation of a new family of periodic mesoporous silicates designated as M41S by using long-chain surfactants as templates [30,31]. Depending on the synthesis conditions, the obtained materials consisted of a hexagonal phase (p6m) referred to as MCM-41, a cubic phase (Ia3d) known as MCM-48, or a non-stable lamellar phase (MCM-50) which can be stabilized by post-synthesis treatment with tetraethyl orthosilicate (TEOS). The success of the Mobil group generated an intense interest among chemists, engineers and materials scientists, especially in the catalysis community. During the last six years, extensive studies have been devoted to the synthesis, characterization, formation mechanism and potential applications of such materials.

Progress in this field has been the subject of several recent reviews [32–38].

Shortly after the disclosure of M41S materials, Stucky and co-workers [39–41] demonstrated that the method can be extended to the synthesis of non-silica-based mesostructured materials. Since then, this particular subject underwent very rapid growth. The present review deals with the synthesis and formation mechanisms of non-silica materials with structures related to the M41S molecular sieves. However, the first part will be concerned with the methodology used in the synthesis of M41S silicates.

### 3. Periodic mesoporous silicates: synthesis and formation mechanisms

The preparation of mesoporous silicates requires at least three ingredients in the appropriate amounts: a source of silica, a surfactant, and a solvent (usually water). Other reagents such as acids, bases, salts, expander molecules and cosolvents may also be used. Depending on the actual synthesis conditions, the final product may be obtained in a few minutes at room temperature, or after hydrothermal treatment, typically at about 100°C for several hours or days.

As for the formation mechanism of M41S silicates, the Mobil group proposed two possible pathways (Fig. 1) [30,31]. The first is that the

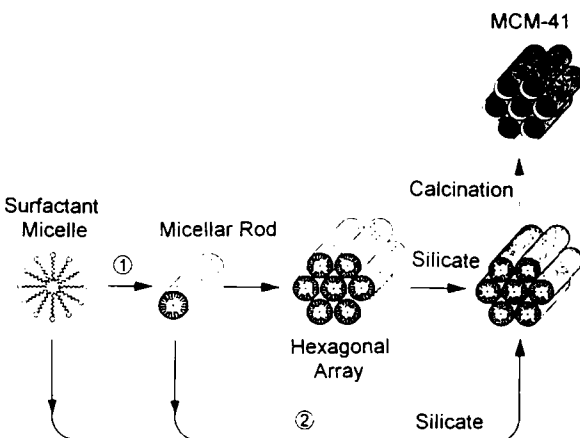


Fig. 1. Mobil group proposed formation pathways of M41S silicates [31].

surfactant molecules self-organize into a liquid crystalline phase which plays the role of a template. The silicate species polymerize into a rigid shell around the hydrophilic parts of such surfactant aggregates. In the second pathway, silicate species in solution play a more active role in directing the formation of the organic–inorganic mesophase through the charge balance with the surfactant ions. These mechanistic proposals arose from the striking similarity between the morphology of M41S silicates and common liquid crystal phases of long-chain surfactants in water solutions. In addition, the successful use of organic expanders to produce structures with larger pores is also indicative of the occurrence of a micelle type chemistry. Further studies by the same group [42–44] and others [40,45] provided ample evidence that no pre-existing liquid crystal phase is required for the formation of M41S silicates. Some of the reasons are as follows: (i) it is possible to make any of the three phases previously mentioned only by changing the amount of silica source, everything else being the same; (ii) mesoporous materials may be made in the presence of surfactant concentrations well below those required for the formation of liquid crystals, and even below the critical concentration for the formation of rod-like micelles; (iii) MCM-41 silicates may be synthesized in the presence of short-chain surfactants such as  $C_{12}H_{25}N(CH_3)_3OH$  which do not form rod-like micelles in water; (iv) MCM-41 and MCM-48 silicates may be formed at temperatures above 70°C where rod-like micelles are not stable.

One of the most important contributions towards the elucidation of the formation mechanism of surfactant templated periodic mesoporous silicates was made by Stucky and co-workers [39,40,46–51]. They proposed the so-called cooperative templating mechanism. This is shown schematically in Fig. 2 using a cationic surfactant ( $S^+$ ) under conditions where the inorganic species are anionic in nature ( $I^-$ ). Prior to silicate addition, the surfactant is in a dynamic equilibrium between spherical or cylindrical micelles and single molecules. Upon addition of a silica source, the multicharged silicate species displace the surfactant counterions to form organic–inorganic ion pairs which reorganize first into a silicatropic mesophase

followed by silica cross-linking. The nature of the mesophase is controlled by the multidentate interaction via the interface packing density. Furthermore, such a cooperative organization process is not limited to ion pairs formed between cationic surfactants ( $S^+$ ) and anionic inorganic species ( $I^-$ ), but can easily be generalized to include three other pathways [39,40]. Pathway  $S^-I^+$  involves the cooperative organization of a cationic inorganic species and an anionic surfactant. The two remaining routes involve interactions between surfactants and inorganic ions with similar charges through the mediation of small ions with the opposite charge. These pathways are referred to as  $S^+X^-I^+$  ( $X^- = Cl^-, Br^-$ ) and  $S^-M^+I^-$  ( $M^+ = Na^+, K^+$ ). Typical syntheses to illustrate each of these pathways have been reported [39,40].

In addition to these mechanisms based on electrostatic interactions, Pinnavaia and co-workers [52–56] introduced a neutral templating mechanism ( $S^0I^0$ ). They used non-ionic surfactants such as primary amine and polyethylene oxide surfactants to prepare silicates with cylindrical nanopores referred to as HMS and MSU-*n*, respectively. Contrary to the above mentioned pathways where the whole organization process is driven by electrostatic interactions, in the presence of neutral surfactants hydrogen bonding becomes the predominant factor. As seen in Fig. 3, the neutral species formed by partial hydrolysis of tetraethyl orthosilicate (TEOS) interacts with the surfactant amine head group via hydrogen bonding. The obtained organic–inorganic complex may be considered as an amphiphile with a very bulky head group. As discussed hereafter, the occurrence of a large head group increases the likelihood for the formation of rod-like micelles with a natural tendency to self-organize into a hexagonal packing. This is followed by condensation of silanol groups and formation of rigid silica walls.

As a first approximation, the morphology of the mesophase can be predicted based on the so-called packing factor  $g = V/a_0l$ , where  $V$  is the total volume of the surfactant chain plus any co-solvent organic molecules between the chains,  $a_0$  is the effective head group area at the micelle surface, and  $l$  is the kinetic length of the surfactant tail

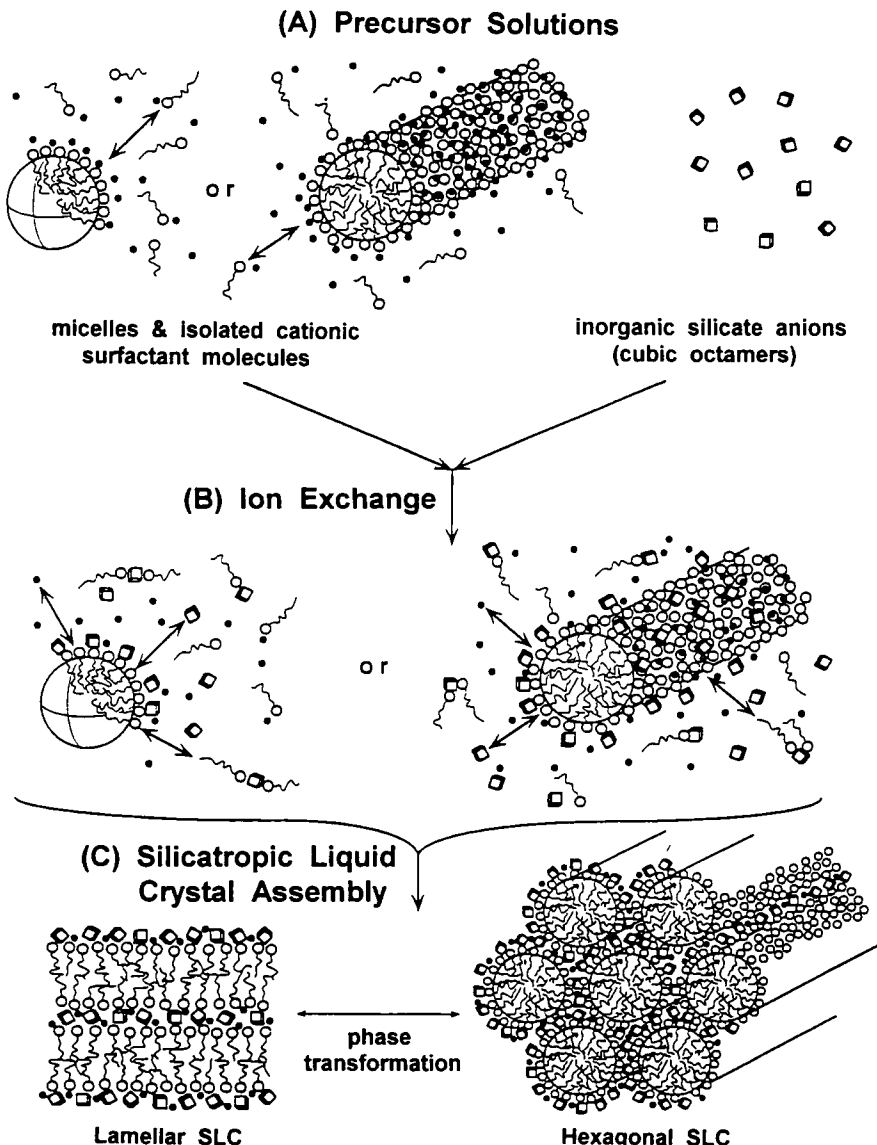


Fig. 2. Cooperative templating mechanism [48].

[57,58]. The nature of surfactant aggregates and the morphology of the corresponding mesophases are related to  $g$  as shown in Table 1 [59].

While all of the above mechanisms have been supported by some experimental results, they are neither exclusive nor definitive. The actual formation mechanism depends on the synthesis conditions. When the concentration of an ionic surfactant is low, the cooperative mechanism is likely to apply. On the other hand, in the presence

Table 1  
Mesophase structure vs. packing factor  $g$  [59]

$g$ Factor	Aggregate	Mesophase
<1/3	spherical micelles	cubic ( $Pm3n$ )
1/3–1/2	cylindrical micelles	hexagonal ( $P6_3/mmc$ )
1/2–1	vesicles or bilayers	hexagonal ( $p6m$ ) cubic ( $Ia3d$ ) lamellar

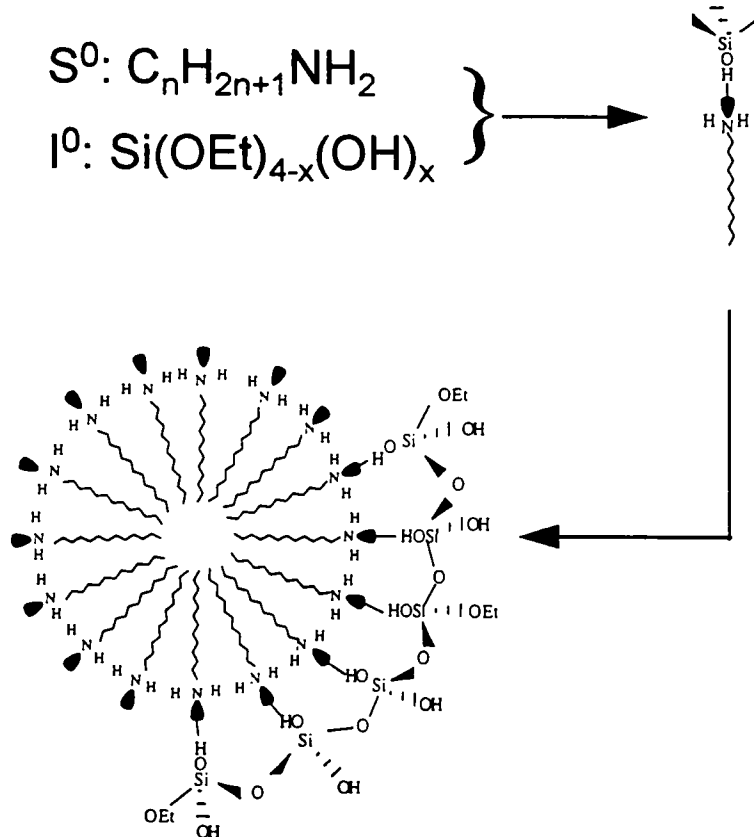


Fig. 3. Neutral templating mechanism [53].

of a high concentration of surfactant, a real liquid crystal templating (LCT) mechanism may take place leading to a material that is in essence an inorganic replica of a preorganized organic array. Notice that, strictly speaking, the pre-existence of an organic liquid crystalline phase, and the formation of a superlattice with matching morphology, are necessary conditions for the occurrence of the LCT mechanism, but they are not sufficient. The work of Attard et al. [60] offers a nice example where both conditions are met, but the organic mesophase was temporarily destroyed by the methanol released from the hydrolysis of tetramethyl orthosilicate. In addition, one must be careful when considering the neutral templating mechanism. Since a long-chain primary amine is a relatively strong base, it may be readily protonated under a wide range of synthesis conditions. As we will show later, in-depth understanding of the

formation mechanism is of paramount importance in developing successful strategies for the synthesis of non-silica materials where the flexibility of the inorganic species to form different phases is not as great as that of silicates.

In addition to the surfactant templating approach discussed above, researchers from Japan succeeded in preparing mesoporous silicates denoted as FSM-16 using a different method [61–64]. They first intercalated a layered silicate (kanemite) by cetyltrimethylammonium cations via ion-exchange with sodium ions. During the subsequent hydrothermal treatment, the silicate layers wind around the intercalated surfactant leading to a highly ordered hexagonal structure.

As shown in Table 2, in addition to the three M41S phases reported by the Mobil group, a number of new mesostructured phases have been discovered. It is worth mentioning that some of

Table 2  
Mesostructured phases synthesized in the presence of surfactants

Phase	Liquid crystal counterpart	Reference
Hexagonal, MCM-41 (p6m)	Yes	[31]
Hexagonal, SBA-2 (P6 <sub>3</sub> /mmc)	Yes	[68, 69]
Cubic, MCM-48 (Ia3d)	Yes	[31]
Cubic, SBA-1 (Pm3n)	Yes	[68]
Lamellar, MCM-50	Yes	[31]
Lamellar (multilamellar vesicle templating)	No	[67]
Lamellar* (vesicle templating)	No	[65]
Lamellar* (concentric growth)	No	[66]

\* Aluminophosphates.

these structures have no counterparts among known lyotropic liquid crystals [65–67], which is a strong argument in favor of the cooperative mechanism. It is also interesting to notice that the 3D-hexagonal structure P6<sub>3</sub>/mmc with cage-shaped pores was discovered as a mesoporous silicate SBA-2 [68] before an identical lyotropic structure was identified in the C<sub>12</sub>EO<sub>8</sub>/water binary system [69].

The pore size of M41S materials can be tuned from ca. 2 to 10 nm using several methods. Pore sizes up to 4–4.5 nm may be achieved by using surfactants with different chain lengths. This method has been tested for all three M41S phases [33, 70] as well as for HMS and SBA-2 [68]. Expander molecules such as 1,3,5-trimethylbenzene (TMB) [31] or linear hydrocarbons [71] may also be used for further pore size enlargement. These molecules increase the size of the surfactant micelles by dissolving into their hydrophobic region. Another method for pore size expansion is known as thermal restructuring [72]. It consists of preparing an MCM-41 silicate at relatively low temperature, e.g. 70°C, then heating it in its mother liquor at high temperature, e.g. 150°C. Recent work in this laboratory showed that this method affords excellent quality silicates with pores up to 6.5 nm wide having very narrow size distribution [73]. MCM-41 prepared at room temperature in the presence of a mixture of divalent surfactant and either a gemini or a alkyltrimethylammonium sur-

factant, then subjected to a mild hydrothermal treatment in water at 373 K, also afforded high quality materials with pore sizes up to 6 nm [59]. The  $d_{100}$  spacing of as-synthesized MCM-41 may also be varied within small ranges in ångstrom [74] or subångstrom [75] increments by using an appropriate co-solvent or a mixture of surfactants. However, it is not clear if the actual pore sizes of calcined materials will follow similar smooth trends. Methods of controlling the pore size through direct manipulation of synthesis conditions were also reported [76, 77].

Mesoporous silicate molecular sieves were characterized by a variety of techniques including XRD, SEM, TEM, adsorption measurements, <sup>29</sup>Si NMR, FTIR, Raman spectroscopy and XANES [33]. XRD patterns of all mesoporous phases are dominated by a limited number of low-angle peaks which can be indexed to a specific crystalline phase. HMS, MSU-*n* and some "MCM-41" silicates exhibit only the 100 peak either because of too small scattering domain sizes [52] or because of poorly ordered pore systems [55, 78–80].

Adsorption measurements indicate that mesoporous silicates have high porosity and very high surface area, often exceeding 1000 m<sup>2</sup> g<sup>-1</sup>. N<sub>2</sub> adsorption–desorption isotherms of MCM-41 [31, 70] and MCM-48 [31, 81] materials are of type IV in the IUPAC classification. For materials with pore sizes below ca. 4 nm, the isotherms are usually reversible and exhibit a sharp step at  $P/P_0$  in the range 0.25 to 0.4 [70, 73] due to capillary condensation within uniform primary mesopores. Samples with larger pores exhibit significant hysteresis loops. The SBA-2 N<sub>2</sub> adsorption isotherm exhibits a H2 hysteresis loop consistent with bottle-shaped pores [68].

Magic angle spinning (MAS) <sup>29</sup>Si NMR was also used extensively for the characterization of M41S silicates [31, 82]. The main observation was that <sup>29</sup>Si NMR spectra were broad and closely resembled those of amorphous silica, a strong indication that the material walls are actually amorphous with a wide range of O–Si–O angles. Such a conclusion was further supported by FTIR [83], Raman [83] and SiK XANES [84] data. This has direct implication for the acidity of M41S type

aluminosilicates [83] and their catalytic properties [85].

#### 4. Synthesis and characterization of non-silica mesostructured materials

##### 4.1. The charge density matching approach

###### 4.1.1. Pioneering work

Stucky and co-workers [39–41] first extended the surfactant templating strategy to the synthesis of non-silica-based mesostructures, mainly metal oxides. Both positively and negatively charged surfactants were used in the presence of water-soluble inorganic species. It was found that for the

formation of an organic–inorganic mesophase to be successful, three conditions should be fulfilled: (i) the inorganic precursor should have the ability to form polyanions or polycations allowing multi-dentate binding to the surfactant; (ii) the polyanions or polycations should be able to condense into rigid walls; (iii) a charge density matching between the surfactant and the inorganic species is necessary to control the formation of a particular phase.

As shown in Table 3 [33,40], all materials but Sb, W and Pb oxides have a strong tendency to form lamellar structures. For tungsten oxide, a hexagonal phase was obtained at a pH of ca. 7. Antimony oxide was prepared in pure cubic (Ia3d), hexagonal and lamellar phases in the presence of  $C_{18}H_{37}(CH_3)_3NBr$ . At an Sb/surfactant

Table 3  
Non-silica mesostructured materials prepared using the charge density matching approach [33,40]

Inorganic precursor	Surfactant	Phase	XRD <i>d</i> spacing (Å) <sup>a</sup>
Sb oxide	$C_{18}H_{37}(CH_3)_3NBr$	cubic (Ia3d)	42.9
Sb oxide	$C_{18}H_{37}(CH_3)_3NBr$	hexagonal	46.0
Sb oxide	$C_{18}H_{37}(CH_3)_3NBr$	lamellar	37.5
W oxide	$C_{16}H_{33}(CH_3)_3NBr$	hexagonal	40.0
W oxide	$C_{16}H_{33}(CH_3)_3NBr$	lamellar	28.3
Zinc phosphate	$C_nH_{2n+1}(CH_3)_3NBr$	lamellar	21.6(10), 23.5(12), 26.0(14), 28.2(16), 30.5(18), 32.5(20)
Alumina	$C_{12}H_{25}C_6H_4SO_3Na$	lamellar	28.9
Pb <sup>2+</sup>	$C_{16}H_{33}SO_3H$	hexagonal	45.8
Pb <sup>2+</sup>	$C_{16}H_{33}SO_3H$	lamellar	38.5
Fe <sup>2+</sup>	$C_{16}H_{33}SO_3H$	lamellar	41.0
Mg <sup>2+</sup>	$C_{12}H_{25}OPO_3H_2$	lamellar	31.0
Mn <sup>2+</sup>	$C_{12}H_{25}OPO_3H_2$	lamellar	28.6
Fe <sup>3+</sup>	$C_{12}H_{25}OPO_3H_2$	lamellar	26.9
Co <sup>2+</sup>	$C_{12}H_{25}OPO_3H_2$	lamellar	30.8
Ni <sup>2+</sup>	$C_{12}H_{25}OPO_3H_2$	lamellar	31.1
Zn <sup>2+</sup>	$C_{12}H_{25}OPO_3H_2$	lamellar	29.6
Al <sup>3+</sup>	$C_{12}H_{25}OPO_3H_2$	lamellar	26.4
Ga <sup>3+</sup>	$C_{12}H_{25}OPO_3H_2$	lamellar	27.2
Fe <sup>2+</sup>	$C_nH_{2n+1}OSO_3Na$	lamellar	21.0(12), 23.0(14), 27.3(16), 30.3(18)
Fe <sup>3+</sup>	$C_nH_{2n+1}OSO_3Na$	lamellar	23.1(12), 26.0(14), 28.1(16), 28.1(18)
Co <sup>2+</sup>	$C_nH_{2n+1}OSO_3Na$	lamellar	20.9 and 39.7(12), 22.8(14), 41.5 and 27.4(16), 28.4(18)
Ni <sup>2+</sup>	$C_nH_{2n+1}OSO_3Na$	lamellar	31.8, 23.5 and 23.2(14), 43.5 and 27.5(16), 24.3(18)
Mn <sup>2+</sup>	$C_nH_{2n+1}OSO_3Na$	lamellar	23.3(14), 42.2 and 28.9(16), 24.3(18)
Tin sulfide	$C_{16}H_{33}(CH_3)_3NBr$	lamellar	25.8

<sup>a</sup> Carbon numbers of the surfactant chains are shown in parentheses.

ratio of 10, adjustment of the pH to 6.7–6.8 resulted in a cubic antimony oxide phase, while at pH 6.2–6.5, a hexagonal phase was obtained. At an Sb/surfactant ratio of 5, only the lamellar phase was formed. Notice that the mesostructured tungsten and antimony oxide phases were formed at lower pH than the corresponding siliceous materials. This is consistent with the charge density matching model, since tungsten and antimony isopolyacids are more acidic than silicic acid.

The formation pathway of non-silica mesostructured materials depends on the nature of the

surfactant charge and that of the inorganic ion involved in the synthesis. Fig. 4 illustrates the four possible combinations in the synthesis of mesostructured surfactant–inorganic biphase arrays, based on electrostatic interactions [39,40].

Regardless of their structure, all the resultant materials collapsed upon calcination. In the case of  $\text{WO}_3$ , it was argued that during calcination, the inorganic framework is possibly reduced by the surfactant, since no oxygen can penetrate into the pores as long as the surfactant is present. The reduced  $\text{WO}_{3-x}$  is then reoxidized to  $\text{WO}_3$ , after

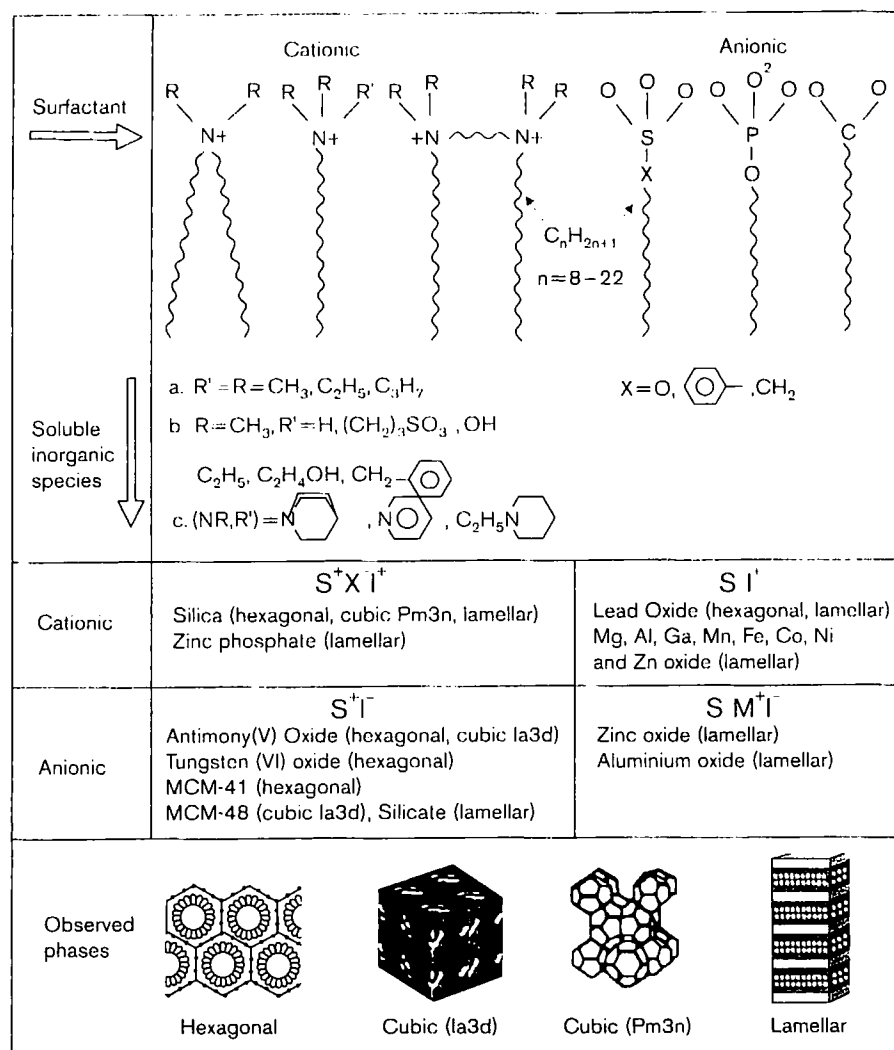


Fig. 4. Synthesis pathways based on electrostatic interactions [39,40].

all the surfactant has been removed. These extensive changes in the oxidation state of the material leads to structural collapse, even if the tungsten species were originally fully condensed in the walls. Calcination of surfactant–antimony oxide mesophases poses similar problems. Other techniques for surfactant removal including tedious calcination procedures with various heating rates and different gas flow compositions, extraction with various solvents, supercritical fluid extraction, and plasma calcination either could not remove the surfactant at all, or resulted in a collapse of the structure [35].

#### 4.1.2. *W and W–Nb oxides: evidence of unconnected inorganic framework*

Stein and co-workers [86,87] independently explored the applicability of the use of surfactants for the synthesis of channel structures with transition metal oxide frameworks. Vanadium, niobium, molybdenum and tungsten oxides were studied. In the case of tungsten oxide, hydrothermal reaction of sodium metatungstate with C<sub>16</sub>TMAOH gave the salt [C<sub>16</sub>H<sub>33</sub>N(CH<sub>3</sub>)<sub>3</sub>]<sub>6</sub>(H<sub>2</sub>W<sub>12</sub>O<sub>40</sub>). Similar material made by Huo et al. [40] showed a surfactant to WO<sub>3</sub> ratio of 1:3, although both preparations were performed at a pH of about 7.

Despite the apparent similarity of TEM micrographs and XRD patterns of this material with those of MCM-41 silicates, UV-visible, IR, and chemical analysis data indicated that the salt contained unconnected Keggin ions H<sub>2</sub>W<sub>12</sub>O<sub>40</sub><sup>6-</sup>. The UV bands for the materials were blue-shifted relative to those of bulk tungsten trioxide and sodium metatungstate, which indicates the presence of isolated metal oxide units. The IR spectrum was also close to that of sodium metatungstate. The Keggin ions were packed in a puckered layer arrangement creating roughly spherical cavities. Attempts to remove the template cations and condense the inorganic portion of the structure invariably led to dense WO<sub>3-x</sub> phases. The formation of Keggin ion salts in the case of tungsten oxide was recently confirmed by Janauer et al. [88].

As in the case of lamellar MCM-50 [89], a stable salt-gel was prepared by reacting the surfactant niobotungstate salt with TEOS. During this treatment Nb–O–Si linkages were formed.

Removal of the cationic surfactant by extraction with acid resulted in porous structures with surface areas up to 265 m<sup>2</sup> g<sup>-1</sup> [86]. However, the material was shown to be XRD amorphous.

#### 4.1.3. *SnO<sub>2</sub>*

The synthesis of mesostructured SnO<sub>2</sub> was achieved by Ulagappan and Rao [90] using SnCl<sub>4</sub> and an anionic surfactant, i.e. sodium di(2-ethylhexyl)sulfosuccinate (AOT). The reaction mixture was composed of 1 SnO<sub>2</sub>:1–2 AOT:1000–2000 H<sub>2</sub>O. XRD showed a single diffraction peak at  $d_0 = 31.5 \text{ \AA}$ . However, the hexagonal nature of the structure was revealed by TEM and atomic force microscopy (AFM). The <sup>119</sup>Sn MAS NMR spectrum consisted of a single peak at  $\delta = -629 \text{ ppm}$ , suggesting that, as in bulk SnO<sub>2</sub> ( $\delta = -604 \text{ ppm}$ ) the coordination of tin in the mesostructured material is octahedral. Similar to the <sup>29</sup>Si NMR signals for M41S silicates, the <sup>119</sup>Sn signal was broad indicating some local disorder around the tin site. The surfactant could not be removed without the collapse of the structure either by extraction with organic solvents or by calcination.

#### 4.1.4. *Ti–P oxide*

Antonelli and Ying [91] prepared the first stable mesoporous transition metal oxide, TiO<sub>2</sub>, using a modified sol–gel method, in which an organometallic precursor was hydrolyzed in the presence of a surfactant. The key factor to obtain the desired hexagonal phase was to control the hydrolysis rate of the precursor, titanium isopropoxide. The condensation reaction should not be too fast to allow the species formed by partial hydrolysis of the titanium alkoxide to combine with the surfactant molecules and self-assemble into a mesostructured arrangement. Since titanium acetylacetone tris-isopropoxide exhibits a diminished hydrolysis rate, the synthesis was carried out in the presence of acetylacetone. Among the many surfactants tested, only alkylphosphates gave rise to a stable hexagonal phase (Fig. 5). For example, after calcination at 623 K, hexagonally packed TiO<sub>2</sub> prepared in the presence of tetradecylphosphate exhibited a BET surface area of 200 m<sup>2</sup> g<sup>-1</sup> and a pore size distribution centered at 32 Å. However, IR

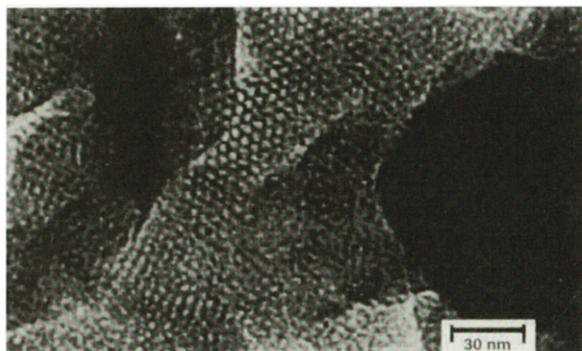


Fig. 5. TEM image of mesoporous TiO<sub>2</sub> prepared in the presence of tetradecylphosphate [91].

spectroscopy revealed a strong absorption band at 1087 cm<sup>-1</sup>, indicating the presence of phosphate ions, even after calcination.

#### 4.1.5. V and V-P oxides: templating vs. intercalation approach

Luca et al. [92] prepared a mesostructured vanadium oxide in two steps. Cetyltrimethylammonium vanadate was first crystallized from water solution. It was then dissolved in alcohol followed by titration with HCl to pH 2.2. The red-brown precipitate (C<sub>20.1</sub>H<sub>48.0</sub>N<sub>1.0</sub>V<sub>2.9</sub>O<sub>11.4</sub>) exhibited a hexagonal structure with  $d=36\text{ \AA}$ . UV-visible, IR and <sup>51</sup>V NMR data indicated that the inorganic walls have a structure resembling vanadium pentoxide rather than unconnected Keggin ions. However, the material was thermally unstable. Janauer et al. [88] prepared a mesolamellar V<sub>2</sub>O<sub>5</sub> surfactant material using dodecyltrimethylammonium bromide (DTABr). Based on recent single-crystal X-ray diffraction studies [93], the dried sample with a  $d$  spacing of 18.9 Å was found to be comprised of discrete dodecavanadate units, V<sub>10</sub>O<sub>28</sub><sup>6-</sup>, associated with four DTA and two H<sub>3</sub>O<sup>+</sup> species, not a continuous metal oxide lattice.

Abe et al. [94] synthesized a hexagonal vanadophosphate using a similar templating method under hydrothermal conditions. The gel composition was VOSO<sub>4</sub>·nH<sub>2</sub>O:0.52 H<sub>3</sub>PO<sub>4</sub>:1.1 alkyltrimethylammonium chloride:92.8 H<sub>2</sub>O. The resulting material had amorphous walls reminiscent of V<sub>2</sub>O<sub>5</sub>–P<sub>2</sub>O<sub>5</sub> glass. Upon calcination at 773 K, the mesostructure was destroyed.

Doi and Miyake [95] reported also on the synthesis of a mesostructured V–P–O compound, using a method similar to that of FSM-16 silicates [61,62]. The starting material, a lamellar VOHPO<sub>4</sub>·0.5H<sub>2</sub>O phase, was intercalated by a long-chain surfactant, such as tetradecyltrimethylammonium chloride. The material was then subjected to a hydrothermal treatment in water. TEM data showed the occurrence of highly ordered hexagonal arrays of pores (Fig. 6). The formation mechanism was suggested to be similar to that described earlier for FSM-16 [63,64]. This study thus demonstrated for the first time that the FSM-16 synthesis route can also be extended to non-silica mesoporous metal oxides.

Recently, Sayari and co-workers [96] used dodecylamine as a template to synthesize mesostructured vanadium oxide. Oxovanadium isopropoxide was hydrolyzed in the presence of the surfactant. Three phases were identified by XRD, i.e. two lamellar phases with  $d_{001}=23\text{ \AA}$  (L1 phase) and 28 Å (L2), and a hexagonal phase (H) with a  $d_{100}$  of 30 Å. While the two lamellar phases could be prepared in pure forms, the H phase was always mixed with the L1 phase. In addition, extensive phase transformations were observed during preparation. For example, the solid separated immediately after formation from a gel of composition 0.5 C<sub>12</sub>H<sub>25</sub>NH<sub>2</sub>:1 VO(O*i*Pr)<sub>3</sub>:7 C<sub>2</sub>H<sub>5</sub>OH:52 H<sub>2</sub>O was comprised of L1 and L2 phases. Upon aging at room temperature, the L2 phase was transformed into the H phase. However, prolonged aging did not lead to pure H. These materials were



Fig. 6. TEM image of mesoporous vanadophosphate [95].

characterized by XRD, SEM, TEM,  $^{13}\text{C}$ ,  $^{15}\text{N}$  and  $^{51}\text{V}$  NMR. There are indications that, in this case, the interactions between the V center and the surfactant head group are not electrostatic in nature, but take place through the formation of a covalent bond [96]. This so-called ligand templating mechanism will be discussed later.

Depending on their synthesis conditions, samples exhibited different morphologies with features such as sheets and plate-like particles consistent with lamellar structure. Moreover, a great diversity of particle shapes from microrods to 3D particles with intricate networks of interconnected rods and micron-sized rose-shaped particles was observed by SEM. These are reminiscent of the growing inventory of particles with unique shapes reported recently for silica and aluminophosphate mesophases prepared in the presence of surfactants [65–67, 97–99].

To rationalize the formation of vanadium oxide–dodecylamine mesostructures, it was suggested that the interactions between vanadium and the amine head group which determine the morphology of the final phase are governed by the acidity of the actual vanadium precursor. As these interactions decrease, the average head group area of the surfactant will decrease, thus leading to a higher  $g$  factor. These events favor the formation of lamellar phases (Table 1). In contrast, stronger interactions would favor the formation of mesophases with higher curvature such as the H phase.

#### 4.1.6. Zirconia and hafnia

Sulfated zirconia is a strongly acidic and oxidizing catalyst with a number of potential applications particularly in the area of hydrocracking and hydroisomerization [100]. Standard preparation methods generate solids with surface areas in the range  $70\text{--}120 \text{ m}^2 \text{ g}^{-1}$ . The idea that zirconia-based materials with much higher surface area may be prepared in the presence of surfactants motivated many researchers to pursue this goal. In addition, mesoporous sulfated zirconia may be prepared in one step by introducing sulfate ions during the synthesis or by using sulfur-containing surfactants.

Sayari and co-workers [101, 102] extended the surfactant templating technique to the synthesis of mesostructured zirconium oxide. The use of

$\text{Zr}(\text{SO}_4)_2$  precursor in the presence of long-chain quaternary ammonium salts or primary amines as templates led to the formation of hexagonal and lamellar  $\text{ZrO}_2$  phases, respectively. Fig. 7 is a typical TEM image of hexagonally packed zirconium oxide [103]. Consistent with the synthesis conditions ( $\text{pH} < 1.5$ ) and energy dispersive X-ray (EDX) analysis data, an  $\text{S}^+ \text{X}^- \text{I}^+$  mechanism where the surfactant–inorganic interaction is mediated by sulfate anions was proposed. The influence of various synthesis parameters such as (i) the  $\text{ZrO}_2$ /surfactant ratio, (ii) the surfactant/water ratio, (iii) the nature of surfactant, (iv) the crystallization temperature, and (v) the crystallization time has been investigated. Both hexagonal and lamellar structures collapsed upon removal of the surfactant either by high temperature calcination or by solvent extraction [102]. However, as shown in Fig. 8, the hexagonal form was successfully stabilized by post-synthesis treatment with potassium phosphate at room temperature followed by air calcination at 623 K. The final product contained significant amounts of phosphorus. It exhibited a surface area exceeding  $500 \text{ m}^2 \text{ g}^{-1}$  [101] and a narrow pore size distribution centered at 1.6 nm.

The authors also studied the effect of addition of a swelling agent, 1,3,5-trimethylbenzene. It was reported that such an agent dissolves in the hydrophobic tail of the surfactant and thus enlarges the micelle size, and hence the pore width of the mesophase. However, in the case of  $\text{ZrO}_2$ , a lamellar structure was obtained instead of a hexagonal phase with larger pores. This was explained using the surfactant packing parameter  $g$  defined earlier. When the swelling agent is added to the system, the effective volume of the surfactant chain increases more rapidly than its effective length, leading to a higher  $g$  value. If the initial  $g$  value is just below 1/2, it is possible that, upon addition of TMB,  $g$  exceeds 1/2 and the hexagonal phase is replaced by a lamellar phase.

Ciesla et al. [104] independently developed a similar approach for the synthesis of zirconium oxide. Using zirconium sulfate and cetyltrimethylammonium chloride, they obtained a thermally unstable hexagonal phase. The material was stabilized by treatment with phosphoric acid. After calcination, the product exhibited a surface area

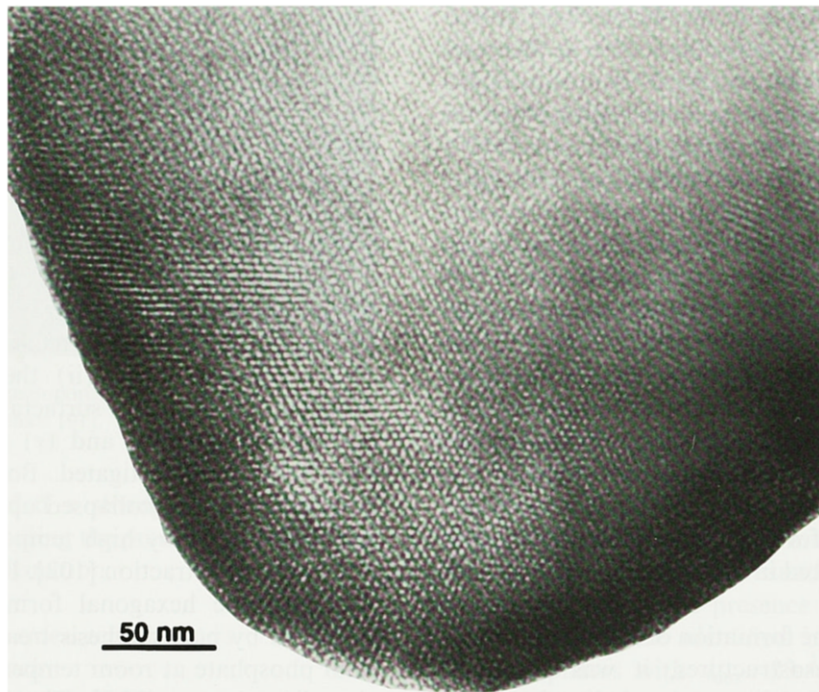


Fig. 7. TEM image of as-synthesized hexagonal zirconium oxide [103].

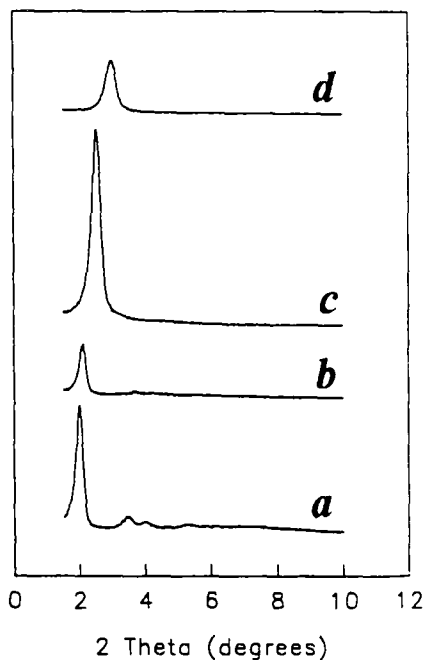


Fig. 8. XRD patterns of (a) as-synthesized hexagonal  $\text{ZrO}_2$ ; (b) after treatment with  $\text{KH}_2\text{PO}_4$ ; (c) after calcination at 623 K for 4 h; (d) after calcination at 773 K for 2 h [101].

of  $230 \text{ m}^2 \text{ g}^{-1}$ . Materials prepared in the presence of  $\text{C}_{18}$  and  $\text{C}_{20}$  surfactants had surface areas of  $320$  and  $390 \text{ m}^2 \text{ g}^{-1}$ , respectively. In addition, a less ordered but stable phase with a surface area of  $280 \text{ m}^2 \text{ g}^{-1}$  was obtained using zirconium isopropoxide and  $(\text{NH}_4)_2\text{SO}_4$  with a large amount of hydrochloric acid.

Knowles and Hudson [105,106] also prepared a mesoporous, high surface area zirconium oxide in a basic medium. At pH 11.4–11.7, zirconium species formed a gel which, through a scaffolding process followed by calcination at 723 K, afforded zirconium oxide samples with surface areas in the range of  $238$ – $329 \text{ m}^2 \text{ g}^{-1}$ . The  $d$  spacings of as-synthesized compounds were independent of the hydrocarbon chain length of the surfactant used, while those of calcined samples varied as a linear function of the chain length. Because this behavior is inconsistent with the above mentioned surfactant templating mechanisms, an alternative mechanism depicted in Fig. 9 was proposed. The positive surfactant ions first exchange with the protons in zirconium hydroxide gel. Subsequently, controlled heating and scaffolding condense the inorganic

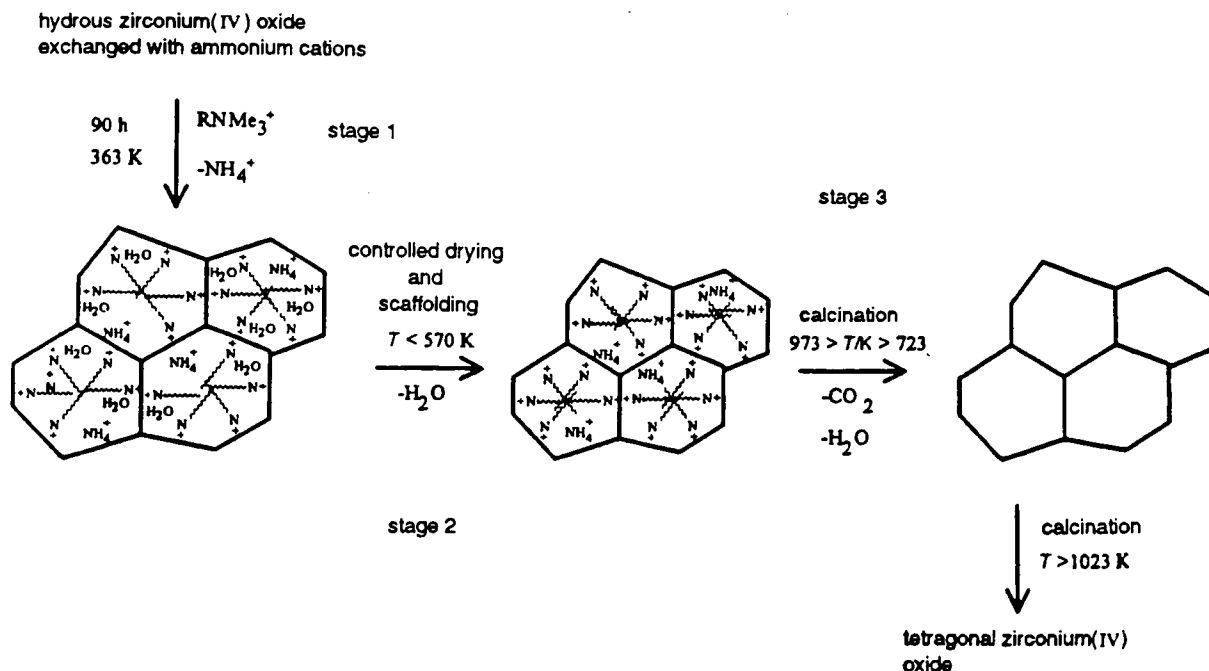


Fig. 9. Schematic diagram of the scaffolding mechanism in long-chain alkytrimethylammonium incorporated  $\text{ZrO}_2$  [105].

structure. The occluded surfactants reduce the surface tension of the water they come into contact with leading, after calcination, to materials with chain length-dependent pore sizes.

Liu and co-workers [38,107,108] used an amphoteric surfactant, cocamidopropyl betaine, with quaternary ammonium and carboxylic acid functionalities to prepare mesoporous  $\text{ZrO}_2$ . The as-synthesized hexagonal material exhibited a  $d_{100}$  spacing of 41 Å. Upon calcination at 350°C, the material had a surface area of  $130\text{ m}^2\text{ g}^{-1}$ . Anionic surfactants such as lauryl sulfate [109,110] and dodecylphosphate [109] were also successfully used for the preparation of mesoporous  $\text{ZrO}_2$ .

Sachtler and co-workers [111] prepared mesoporous  $\text{ZrO}_2$  using Zr isopropoxide in the presence of hexadecane amine as template. As in the case of titanium oxide discussed above, the hydrolysis rate of zirconium species was decreased by adding acetylacetone. After synthesis, the surfactant was successfully removed by extraction with ethanol at 80°C. A material with a BET surface area up to  $347\text{ m}^2\text{ g}^{-1}$  and a pore radius of 18.5 Å was

obtained. As discussed later, the sulfated form exhibited interesting catalytic properties.

Recent work in our laboratory dealt with the preparation of porous hafnium oxide using the surfactant templating approach [112]. Hafnium chloride was first hydrolyzed in water, then mixed with a solution of CTAB and ammonium sulfate. After adjusting the pH of the gel to ca. 2, a hexagonal-like phase was formed at room temperature or after hydrothermal treatment at 373 K (Fig. 10). The material obtained at 373 K was found to be stable after calcination at 773 K. A porous material with a surface area of  $204\text{ m}^2\text{ g}^{-1}$  and an average pore size of 1.1 nm was obtained. Since hafnium oxide is also useful for the preparation of strong acid catalysts, this approach thus provides a straightforward method for obtaining high surface area materials.

In terms of potential applications, Schüth [35] found that sulfated mesoporous zirconia was more active than H-ZSM-5 in the disproportionation of ethylbenzene which requires strongly acidic sites. These catalysts were also found to be up to one

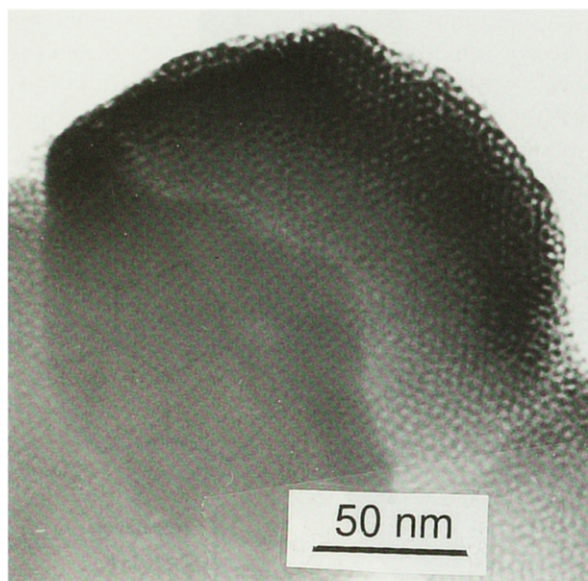


Fig. 10. TEM image of as-synthesized hexagonal hafnium oxide [112].

order of magnitude more active than H-ZSM-5 and commercial sulfated zirconia in the isomerization of n-butane. As in conventional sulfated zirconia [100], Sachtler and co-workers [111] found that treatment of mesoporous zirconium oxide with  $H_2SO_4$  improves its thermal stability. The mesoporous structure was preserved up to a calcination temperature of 700°C, while the amorphous  $ZrO_2$  walls underwent crystallization into a tetragonal phase. In contrast, non-sulfated zirconia lost its porosity above 300°C. The material did not show higher activity in n-butane isomerization compared to conventional sulfated zirconia catalysts. However, as shown in Table 4, the beneficial effect of the presence of mesopores was best

demonstrated in the alkylation of 1-naphthol with 4-*tert*-butylstyrene.

#### 4.1.7. Manganese oxide

Suib and co-workers [113] prepared mixed-valent semiconducting mesoporous manganese oxide with hexagonal (MOMS-1) and cubic (MOMS-2) structures. Fig. 11 is a TEM image of calcined MOMS-1 along with the corresponding

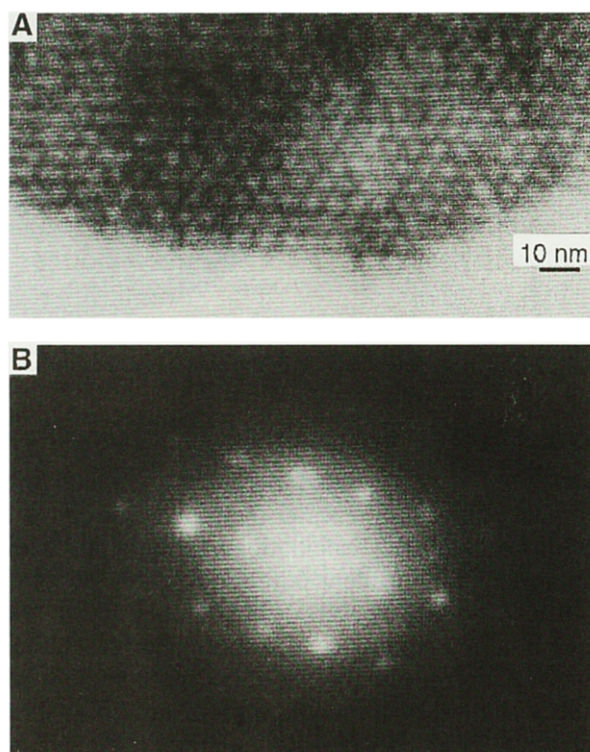


Fig. 11. (A) TEM image of mesoporous hexagonal manganese oxide; (B) electron diffraction pattern [113].

Table 4  
Alkylation of 1-naphthol with 4-*tert*-butylstyrene [111]<sup>a</sup>

Catalyst	1-Naphthol	4- <i>t</i> -Butyl styrene	<i>p</i> -Alkylated product	<i>o</i> -Alkylated product
None	34.0	61.2	0	0
SZ <sup>b</sup>	31.7	57.1	7.4	0
MSZ <sup>c</sup>	19.3	44.1	15.1	10.1

<sup>a</sup> Reaction conditions: 0.15 mol 1-naphthol, 0.3 mol 4-*tert*-butylstyrene,  $t=6$  h,  $T=120\text{--}130^\circ\text{C}$ .

<sup>b</sup> Standard sulfated zirconia.

<sup>c</sup> Mesoporous sulfated zirconia.

electron diffraction pattern. The synthesis of such materials involved the formation of layered  $\text{Mn}(\text{OH})_2$  followed by interaction with an aqueous solution of CTAB, mild oxidation and calcination in air at 823 K. The nature of the interactions between the  $\text{Mn}(\text{OH})_2$  precursor and the surfactant has not been well established. The obtained materials exhibited a number of interesting characteristics. The walls of mesopores were thick (1.7 nm) and robust, which imparted the materials with unusually high thermal stability compared to octahedral manganese oxide molecular sieves [114]. In addition, the walls were comprised of microcrystallites of dense phases of  $\text{Mn}_2\text{O}_3$  and  $\text{Mn}_3\text{O}_4$  with the primary structural units being  $\text{MnO}_6$  units. The average oxidation number of calcined MOMS-1 was found to be 3.55, corresponding to the occurrence of  $\text{Mn}^{2+}$ ,  $\text{Mn}^{3+}$  and  $\text{Mn}^{4+}$  with proportions 1:21.7:30.2 as determined by analytical techniques.

The conductivities of calcined MOMS-1 and MOMS-2 were  $2.28 \times 10^{-6}$  and  $8.13 \times 10^{-6}$   $(\Omega \text{ cm})^{-1}$ , respectively. In comparison, synthetic todorokite, which is a microporous mixed-valent manganese oxide with similar average oxidation number (3.5) as MOMS-1 (3.55), has a conductivity of only ca.  $2 \times 10^{-7} (\Omega \text{ cm})^{-1}$ , indicating that the special structural features of MOMS-1 may be at the origin of the improved conductivity. In addition, MOMS-1 was found to be active in partial oxidation of cyclohexane and n-hexane in the presence of dilute  $\text{H}_2\text{O}_2$ .

#### 4.1.8. Metal sulfides

Compared to metal oxides, less attention has been paid to the synthesis of mesostructured metal sulfides [40,115]. The only systematic work was reported by Anderson and Newcomer [115]. They applied the surfactant templating approach to the preparation of Mo, W, Co, Fe, Zn, Ga, Sn and Sb sulfides. All of the products were lamellar and consisted of bilayers or interdigitated layers of surfactant molecules sandwiched between metal sulfide lamellae.

Braun et al. [116] prepared nanostructured CdS templated directly by a hexagonal mesophase of oligoethylene oxide oleyl ether in a cadmium acetate aqueous solution. Precipitation of CdS by flowing  $\text{H}_2\text{S}$  led to an organic–inorganic composite

with all the architectural characteristics of the precursor mesophase. This is most likely the closest available example of a real LCT mechanism, for the nature of the mesophase never changed throughout the synthesis. The preparation of analogous composites was successful with CdSe, but not with PbS, indicating the importance of ion-amphiphile interactions in the formation of the superlattice structure.

Recently, Li et al. [117,118] reported on the synthesis of mesostructured tin(IV) sulfide using CTAB as the template. In the presence of CTAB/ $\text{SnCl}_4$  ratios higher than 0.33, a lamellar phase with a basal spacing of 25.5 Å was obtained.  $^{119}\text{Sn}$  MAS NMR consisted of one single line at  $\delta = 52.7$  ppm, indicating that contrary to  $\text{SnS}_2$  ( $\delta = -764$  ppm) and  $\text{SnO}_2$  ( $\delta = -604$  ppm), tin in the inorganic layers was tetrahedrally coordinated. Based on the  $d$  value and on chemical analysis ( $\text{S/Sn} = 2.5$ ; 58.5 wt% organic material), it seems that this phase is a precipitated salt with the formula  $(\text{SnS}_{2.5})(\text{C}_{19}\text{H}_{42}\text{N}^+)$ . This is reminiscent of lamellar alkyl dihydrogenophosphate materials prepared in the presence of decylamine [65] and dodecylamine [119] with  $d$  spacings of 19.5 and 22.5 Å, respectively. At much lower CTAB concentration, Li et al. [118] obtained a mesostructured phase with  $d$  spacing of 39.2 Å. This material exhibited only one  $^{119}\text{Sn}$  MAS NMR peak at  $\delta = -520$  ppm, indicating that, in this case, Sn is hexacoordinated. It is interesting to notice that Sn in mesoporous tin oxide was also found to be in an octahedral environment [90].

#### 4.1.9. Aluminophosphates and aluminoborates

With the ultimate goal of preparing stable mesoporous aluminophosphates, several research groups attempted to apply the supramolecular templating technique. Using a gel composition of 1 C<sub>n</sub>TBAB:1  $\text{P}_2\text{O}_5$ :0.3  $\text{Al}_2\text{O}_3$ :1.6 TMAOH:15  $\text{H}_2\text{O}$ , Fyfe et al. [120] obtained a series of layered aluminophosphates for  $n$  values higher than 12. Ozin and co-workers [65,121–123] carried out the synthesis in a non-aqueous medium and also obtained mesolamellar aluminophosphates. The composition of the synthesis gel used was 14 TEG:0.9  $\text{Al}_2\text{O}_3$ :2.5  $\text{H}_2\text{O}$ :1.8  $\text{P}_2\text{O}_5$ :3.0  $\text{C}_{10}\text{H}_{21}\text{NH}_2$ , where TEG denotes tetraethylene glycol. Scanning electron microscopy showed that, in some parts of

the resulting lamellar materials, there existed micrometer scale surface patterns, including bowl, honeycomb, and quilted shapes with superimposed finer columnar, sphere, mesh, and pore-like structural features (Fig. 12). The origin of these patterns was explained based on a proposed vesicle templating mechanism along with a “cellular” model (Fig. 13). The multifunctional role of TEG was emphasized [65,123]. Among these functions, TEG acted as a solvent to enable the self-assembly of the vesicle template, a polydentate ligand to  $\text{Al}^{3+}$ , a co-surfactant for control of the bilayer curvature, a demixing agent to promote surfactant–TEG phase separation and patterning of vesicles, and as artificial ion-channels to facilitate

the transport of (TEG) $\text{Al}^{\text{III}}$  ionophores through vesicle bilayers. The micrometer scale patterns obtained mimic some natural diatom and radiolaria microskeletons. Templating by amphiphilic vesicles thus extended the surfactant templating principle to the next level of the hierarchical ladder, carrying the pattern to the micrometer scale.

Gao et al. [124] also prepared a series of lamellar aluminophosphates in non-aqueous medium. They used the following gel compositions:  $(\text{iPrO})_3\text{Al}:1.8 \quad \text{H}_3\text{PO}_4:3.4 \quad \text{C}_n\text{H}_{2n+1}\text{NH}_2:3.4$   $\text{C}_m\text{H}_{2m+1}\text{OH}:13.8 \quad \text{EG}:1.7 \quad \text{H}_2\text{O}$  ( $n=6, 8, 10, 12$ ;  $m=4-8$ ; EG = ethylene glycol). All products exhibited an Al/P ratio of 2 to 1, and their  $d_{001}$  spacings increased from 22.5 to 34.7 Å when  $n$  increased from 6 to 12.

Sayari and co-workers [66,119,125,126] followed another path to the synthesis of mesolamellar aluminophosphates. They used  $\text{Al}_2\text{O}_3$ ,  $\text{H}_3\text{PO}_4$  and primary or tertiary amines as surfactants in aqueous media.  $^{15}\text{N}$  and  $^{13}\text{C}$  CP MAS NMR data showed that the occluded surfactant was protonated. Attempts were made to prepare  $\text{AlPO}_4$  materials with three-dimensional rather than lamellar structure by modifying the composition of the starting synthesis mixture. The systematic approach consisted of changing the amount relative to  $\text{P}_2\text{O}_5$  of all other starting materials one at a time. In addition, the effects of alkylamine chain length, crystallization temperature and time were also investigated. However, only lamellar phases were obtained.  $^{27}\text{Al}$  NMR data for samples prepared using the following compositions:  $\text{H}_3\text{PO}_4:y \text{Al}_2\text{O}_3: \text{C}_{12}\text{H}_{25}\text{NH}_2:60 \text{H}_2\text{O}$  with  $0.6 \leq y \leq 2$  revealed three different Al species in the inorganic layer, namely a tetrahedral Al bonded to four P atoms via oxygen bridges, an octahedral framework Al in interaction with water molecules, and the unreacted alumina. A broad  $^{31}\text{P}$  signal at ca. –13 ppm was interpreted as a combination of tetrahedral P sites bonded to  $(4-x)$  Al through oxygen bridges and to  $x$  hydroxyl groups ( $x=1$  or 2). The connectivity between Al and P was found to be dependent on the synthesis parameters.

TEM studies [66] indicated that in some samples, apart from the simple lamellar packing (Fig. 14a), there were extended areas comprised of

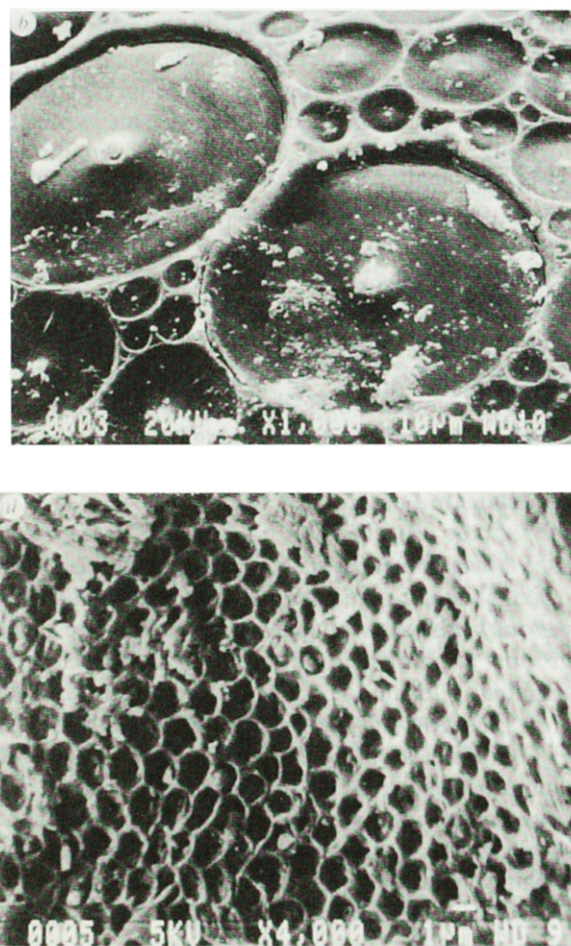


Fig. 12. Examples of SEM images of decylamine mesolamellar aluminophosphate with different surface morphologies [65].

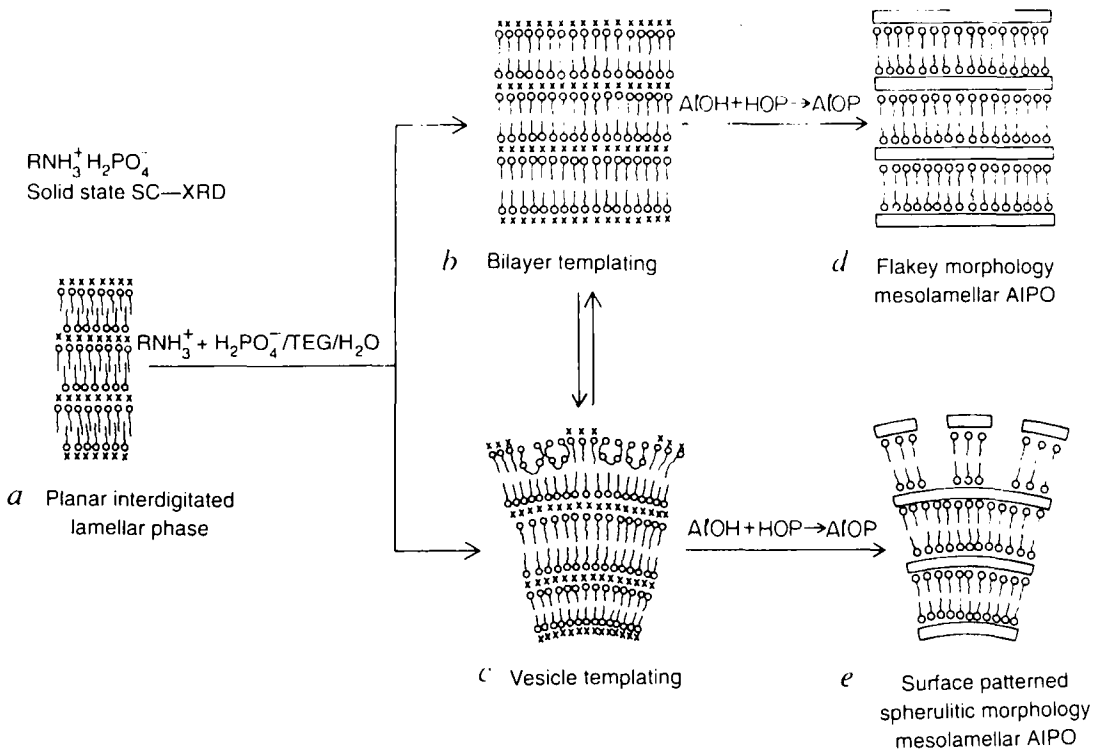


Fig. 13. Schematic illustration of proposed patterning mechanism in mesolamellar aluminophosphates [65].

a unique hexagonal-like packing of alternating concentric dark and bright rings (Fig. 14b and c). As shown schematically in Fig. 14d, the circular fringes were interpreted as the edge projections of cylindrical layers of inorganic  $\text{AlPO}_4$  materials separated by cylindrical vesicles of surfactant, all wrapped around a single rod-like micelle. It is believed that this new mesophase has no equivalent among known surfactant liquid crystal phases.

Two research groups succeeded recently in preparing mesostructured aluminophosphate with hexagonal structures. Kimura et al. [127] proceeded via hydrothermal treatment of a gel with the following composition:  $\text{Al}_2\text{O}_3:\text{P}_2\text{O}_5: \text{C}_{16}\text{TMACl}:2 \text{ TMAOH}:65 \text{ H}_2\text{O}$ . More recently, Feng et al. [128] used the fluoride route to synthesize mesostructured hexagonal and lamellar  $\text{AlPO}_4$  in the presence of CTAB at a pH of ca. 8.3. Both the aluminum and the base sources were found to play a key role in the synthesis of periodic materials. In the lamellar phase, Al was mainly tetrahedrally coordinated, whereas both tetrahedral and

octahedral Al sites were present in the hexagonal mesophase. The thermal stability of such materials is yet to be proven.

Chakraborty et al. [129] extended the use of the surfactant templating approach to the synthesis of mesostructured silicoaluminophosphates (SAPOs). Hydrothermal treatment of a gel with the following composition: 71.2  $\text{P}_2\text{O}_5$ :26.8  $\text{Al}_2\text{O}_3$ :1.0  $\text{SiO}_2$ :31.5 CTAB:6082  $\text{H}_2\text{O}$  at a pH of ca. 2.5 for 48 h at 383 K afforded thermally stable mesoporous SAPOs. All materials exhibited surface areas exceeding  $900 \text{ m}^2 \text{ g}^{-1}$  with pore size distributions centered around 3 nm. NMR data showed that both P and Al were in tetrahedral sites, whereas there were four different Si sites with 1, 2, 3 and 4 Al, but no P in their second coordination shells. The structure of these SAPOs is still uncertain. Indeed, though the low angle region of the XRD spectra resembles typical MCM-41 spectra with the highest  $d$  distance being comparable to the pore size (2.8 vs. 3 nm), there were two strong unknown peaks at  $2\theta = 2.039$  and 2.074 nm.

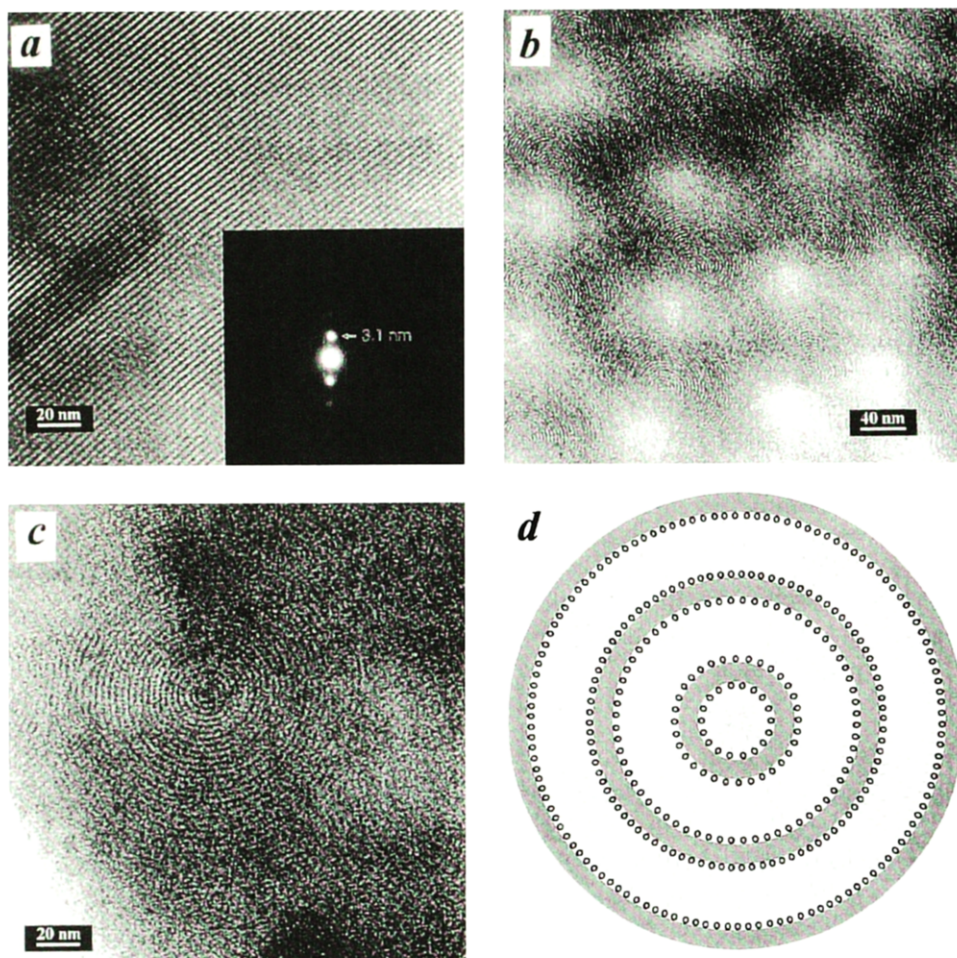


Fig. 14. TEM images of dodecylamine mesolamellar aluminophosphate: (a) lamellar structure; (b) hexagonal-like arrays of concentric rings; (c) close-up showing concentric rings; (d) schematic illustration of edge-on view of the inorganic–organic bilayers coaxially wrapped around a rod-like micelle [66].

Ayyappan and Rao [130] prepared hexagonal, cubic and lamellar mesostructured aluminoborates in the presence of dodecylsulfate at different pH. Surfactant removal from the hexagonal phase by ethanol extraction gave rise to a porous material with a surface area of  $470 \text{ m}^2 \text{ g}^{-1}$  and a pore diameter of  $32 \text{ \AA}$ . Moreover, the XRD  $d_{100}$  spacing could be shifted from  $41.7$  to  $56.6 \text{ \AA}$  by addition of linear hydrocarbons as expander molecules.

#### 4.2. Alumina: $S^0I^0$ vs. $S^-I^+$ approach

Aluminas are important catalysts and catalyst supports for a large number of industrial processes.

One of the major problems related to the use of alumina-based catalysts is the deactivation by coke formation and pore plugging which may be exacerbated by the presence of micropores. Thus, synthesis of aluminas with porosity comparable to M41S silicates would be of practical significance.

Pinnavaia and co-workers [52, 55, 131] used the neutral templating approach to synthesize mesoporous alumina with hexagonal-like structure. Three forms of aluminas, denoted as MSU- $n$ , with  $n=1-3$ , were prepared by the hydrolysis of tri-sec-butoxyaluminum at ambient temperature in the presence of non-ionic polyethylene oxide surfactants such as Tergitol® C<sub>11-15</sub>[EO]<sub>9</sub>,

$C_{11-15}[EO]_{12}$ ,  $C_{11-15}[EO]_{20}$ , Igepal<sup>®</sup> C<sub>12</sub>Ph[EO]<sub>18</sub>, Triton<sup>®</sup> C<sub>8</sub>Ph[EO]<sub>8</sub>, C<sub>8</sub>Ph[EO]<sub>10</sub> and Pluronic<sup>®</sup> [PEO]<sub>13</sub>[PPO]<sub>30</sub>[PEO]<sub>13</sub>. Consistent with the occurrence of a disordered array of mesopores as observed by TEM, the materials obtained exhibited only a single XRD peak. The Barrett–Joyner–Halender (BJH) [132] analysis of the N<sub>2</sub> desorption isotherm gave a narrow pore size distribution with a mean pore radius ranging from 2.4 to 4.7 nm depending on the surfactant used. Both as-synthesized and calcined samples exhibited three <sup>27</sup>Al MAS NMR signals at  $\delta=0$ , 35, and 75 ppm. These lines were assigned to six-, five- and four-coordinated Al species, respectively [133]. In the as-synthesized material the six-coordinated species was dominant, but after dehydration and dehydroxylation at 773 K both the four- and five-coordinated centers increased at the expense of the six-coordinated species. The presence of five-coordinated aluminum species is especially important as they may prove to be of catalytic significance as Lewis acid sites. It was also mentioned that non-layered alumina can be synthesized using a neutral aluminum alkoxide precursor and an alkyl amine surfactant.

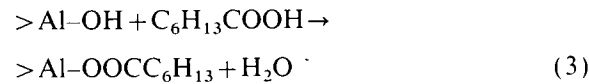
Synthesis of alumina mesophase was also achieved by Yada et al. [134] using aluminum nitrate nonahydrate as the aluminum source and sodium dodecyl sulfate as the templating agent. The precipitation of alumina from an initially homogenous solution was achieved using the hydrolysis of urea to adjust the pH above 5.5. The as-synthesized material exhibited a hexagonal structure. However, upon thermal treatment, the pore structure was much less ordered. No information about the surface area was reported.

Vaudry et al. [135] published an extensive study on the synthesis of mesoporous alumina. The materials were synthesized by reacting aluminum alkoxides and long-chain carboxylic acids with controlled amounts of water in the presence of low molecular weight alcoholic solvents. Calcination of these materials afforded aluminas with specific surface areas as high as 710 m<sup>2</sup> g<sup>-1</sup> and randomly ordered pores with narrow pore size distributions centered at 20 Å and no micropores. The formation mechanism of mesoporous alumina was also discussed. When aluminum alkoxide is

hydrolyzed in an organic solvent with controlled amounts of water, two reactions may occur:



The freshly precipitated aluminum hydroxide interacts swiftly with carboxylic acid (Eq. (3)), thus preventing its transformation into pseudo-boehmite:



The ability for carboxylate ligands to coordinate with one or two aluminum sites on very small clusters of AlOOH was proposed to be at the origin of the rapid formation of alumina mesophases.

The materials were characterized by <sup>1</sup>H, <sup>13</sup>C and <sup>27</sup>Al MAS NMR. Results similar to those of Bagshaw and Pinnavaia [131] were obtained. Table 5 shows typical properties of the alumina mesophases prepared in 1-propanol. While the *d* spacings of as-made materials showed some correlation with the carbon number of the surfactant chain, their calcined forms exhibited no such trend. After calcination, not only the *d* spacings increased significantly, but their order was actually opposite to that of the as-made samples. In addition, the BJH pore size was found to be almost independent of the carbon chain length of the surfactant. It was argued that calcination of alumina mesophases involves a lowering of the local order and the symmetry of the aluminum local environment as inferred by the coexistence of four-, five-, and six-fold coordinated aluminum species, broad <sup>27</sup>Al NMR line shapes, and substantial amounts of NMR-invisible aluminum sites. This is in contrast to the case of silica-based mesoporous materials, where the coordination of the silicon atoms was unaffected by calcination.

It would be interesting to compare the adsorption behavior of MSU-*n* alumina with that of alumina prepared in the presence of alkyl carboxylic acids (Fig. 15). The MSU-3 alumina exhibited an adsorption isotherm with a hysteresis loop and a broad but well-defined adsorption step. It was suggested that some necking of the pore structure is present as indicated by the sharp curvature in

Table 5

Characterization of the porosity of alumina mesophases prepared in 1-propanol [135]

Sample No.	Surfactant used	<i>d</i> spacing (Å)		BET SSA <sup>a</sup> ( $\text{m}^2 \text{g}^{-1}$ )	PD (Å) <sup>a</sup>
		As-made	Calcined		
CA383	C <sub>5</sub> H <sub>11</sub> COOH	24	53	530	21
LA383	C <sub>11</sub> H <sub>23</sub> COOH	29	47	710	19
SA383	C <sub>17</sub> H <sub>35</sub> COOH	36	43	700	21

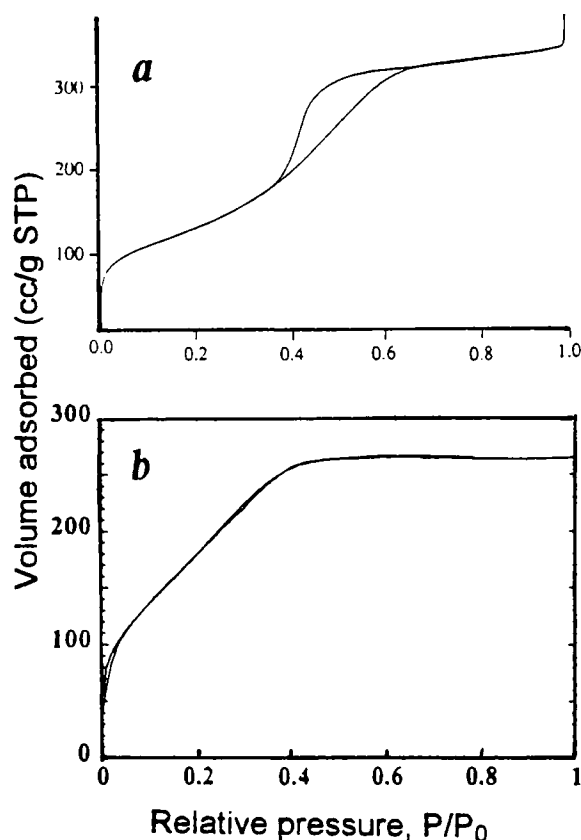
<sup>a</sup> BET SSA: BET specific surface area; PD: pore diameter.

Fig. 15. Nitrogen adsorption–desorption isotherms for mesoporous aluminas: (a) MSU-3 sample prepared via a neutral templating mechanism in the presence of Pluronic 64L (BASF) surfactant [131]; (b) LA383 sample prepared in the presence of caproic acid using 1-propanol as solvent [135].

the desorption curve of the hysteresis loop. The BET surface area was found to be  $430 \text{ m}^2 \text{ g}^{-1}$ . In contrast, the LA383 alumina showed a reversible isotherm, similar to that of MCM-41. Although the pore size was only  $19 \text{ \AA}$ , much smaller than

the  $48 \text{ \AA}$  of MSU-3, its surface area was as high as  $710 \text{ m}^2 \text{ g}^{-1}$ . These differences are similar to those found between HMS and MCM-41 silicates [52, 55, 136].

#### 4.3. Nb and Ta oxides: ligand-assisted templating approach

As indicated in the Introduction, one of the main steps in the synthesis of periodic mesoporous materials is the interaction between the surfactant and the inorganic species in solution. So far, we have described two types of interaction. The first was electrostatic in nature with the formation of ionic bonds either directly or through the mediation of counterions. The second was a van der Waals interaction between non-charged organic surfactants and inorganic species. At this point one may envisage an organic–inorganic interaction that results in a covalent bond. Indeed, this so-called ligand-assisted templating (LAT) approach has been successfully used by Ying and co-workers for the synthesis of novel mesoporous transition metal oxides [137–140].

The method may be illustrated using  $\text{Nb}_2\text{O}_5$  as an example. The synthesis was achieved via the condensation of an organometallic precursor in which the propagating niobium alkoxide moiety is chemically linked through an Nb–N covalent bond to a long-chain amine surfactant molecule [137, 139]. As schematically depicted in Fig. 16, the initial reaction between the amine and  $\text{Nb}(\text{OEt})_5$  was conducted in the absence of water to ensure that a covalent bond between the Nb and the surfactant is formed prior to condensation of the inorganic species. The resultant complex was then allowed to react with water, leading to a

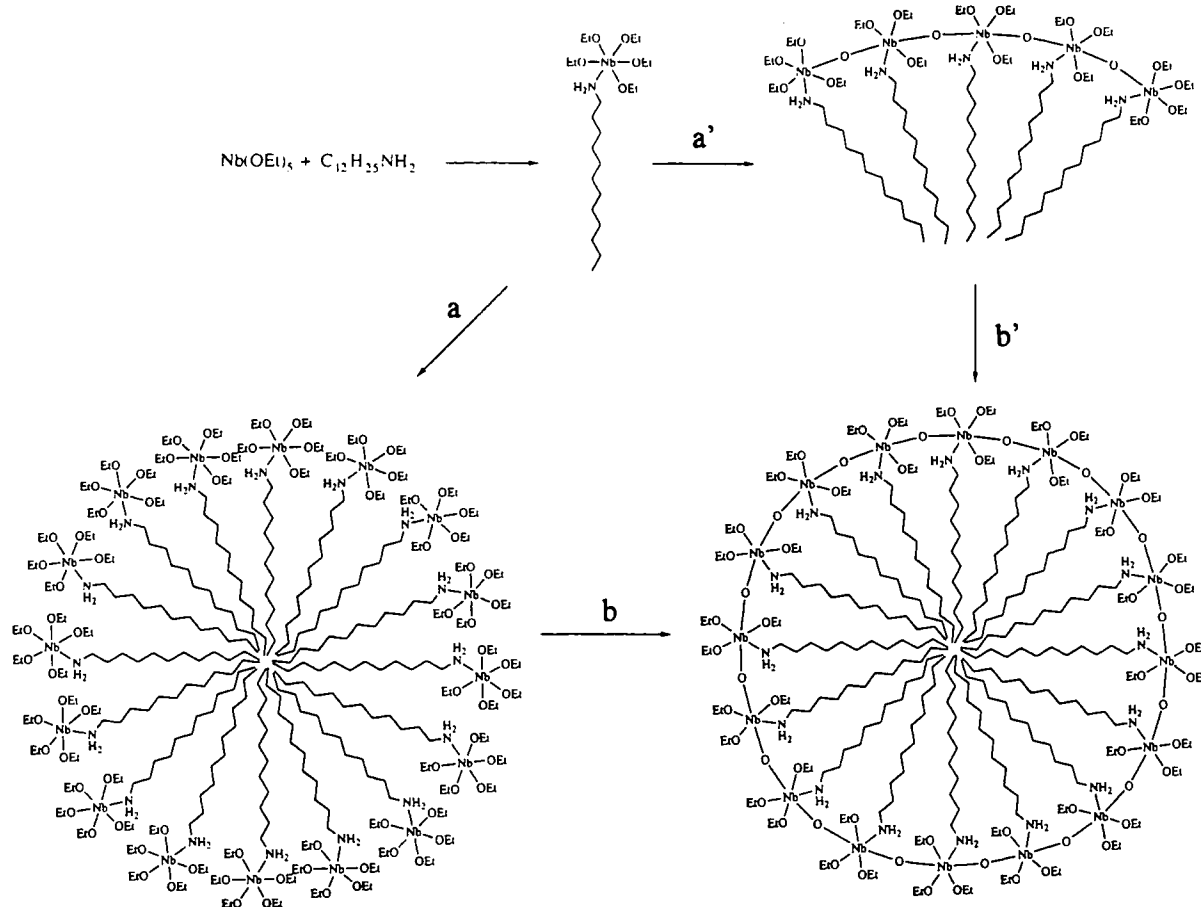


Fig. 16. Schematic representation of possible pathways for the synthesis of mesostructured niobium oxide under a ligand-assisted templating mechanism [137].

thermally stable, hexagonally packed mesoporous niobium oxide (denoted Nb-TMS1). Fig. 17 provides typical TEM images of mesoporous Nb-TMS1 prepared in the presence of tetradecylamine [137].

A key step in the LAT mechanism is the occurrence of a covalent bond between the transition metal Me and N of the surfactant. This proposal was inferred from solution and solid state  $^{15}\text{N}$  MAS NMR studies conducted on 100%  $^{15}\text{N}$  enriched dodecylamine niobium ethoxide precursor in  $[\text{D}_8]\text{toluene}$  and Nb-TMS1 synthesized from  $^{15}\text{N}$  labelled dodecylamine [137]. The presence of substantial line broadening, attributable to the  $^{93}\text{Nb}$  quadrupole ( $I=9/2$ ) in  $^{15}\text{N}\{^1\text{H}\}$  NMR spectra of both the precursor complex in

$[\text{D}_8]\text{toluene}$  and the as-synthesized Nb-TMS1 was interpreted as strong evidence of the occurrence of an N–Nb covalent bond in both substances. The difference in chemical shifts between the precursor complex and pure dodecylamine in  $[\text{D}_8]\text{toluene}$  (ca. 6 ppm) was virtually identical to the difference between as-synthesized solid Nb-TMS1 and pure solid dodecylamine. This suggests that nitrogen in Nb-TMS1 remained bonded to Nb throughout the course of the synthesis process. A similar study conducted on tantalum oxide Ta-TMS1 led to identical conclusions.

Ying and co-workers [139] undertook a systematic study of the synthesis conditions of mesoporous niobium oxide molecular sieves. A screening study of surfactants with different head

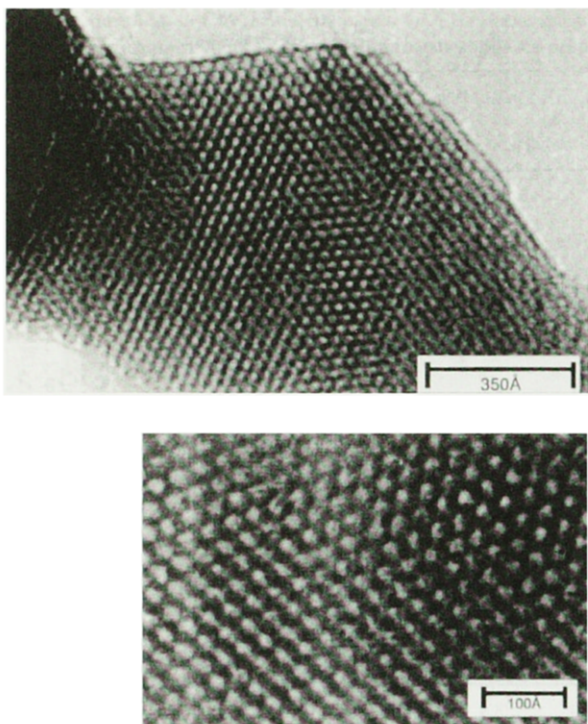


Fig. 17. TEM images of as-synthesized mesoporous niobium oxide prepared via the ligand-assisted templating approach [137].

groups was performed and primary amines and phosphates were found to yield discernible hexagonal materials. In general, surfactants with stronger basicity or greater hapticity led to better quality materials. It was argued that an X-type ligand which is capable of forming a discrete  $\sigma$  bond with the Nb center is required rather than a Lewis basic L-type ligand. It was also found that, with increasing surfactant/metal ratios, a three-dimensional hexagonal  $P6_3/mmc$  (Nb-TMS2) and a layered (Nb-TMS4) phase could be formed in addition to the ordinary two-dimensional MCM-41 type hexagonal phase. A cubic  $Pm3n$  phase (Nb-TMS3) was also obtained under certain conditions. The surfactant was removed by extraction with ethanol in the presence of an acid, leading to a porous metal oxide. When dodecylamine was used as the template, Nb-TMS1 with surface area as high as  $434 \text{ m}^2 \text{ g}^{-1}$  and narrow pore size distribution centered at  $27 \text{ \AA}$  was obtained.

As shown in Fig. 18, the different phases

obtained were rationalized based on the solution chemistry of a mixture of amine and  $\text{Nb(OEt)}_5$ . The bis(amine) adduct (species 5) favors the layered and possibly  $P6_3/mmc$  phases via pathway D, while complexes 3 and 4 promote the hexagonal phase through pathways B and C. The conditions leading to the formation of the  $P6_3/mmc$  phase (1.5:1 dodecylamine to  $\text{Nb(OEt)}_5$  with no ethanol) are favorable to the occurrence of both species 4 and 5, indicating a possible link between these species and the 3D mesophase. Excess ethanol inhibits pathway D and favors pathway A. This explains why no layered, 3D hexagonal ( $P6_3/mmc$ ) or cubic phases were formed in the presence of alcohol.

The authors were also able to prepare high quality hexagonal materials from very dilute solutions of surfactant in alcohols and stoichiometric amounts of water. Since under such conditions the formation of micelles is highly unlikely, it was concluded that neither preformed micelles nor charge density matching is required for self-assembly.

The effects of the surfactant chain length and the swelling agent TMB were also investigated. Increasing the surfactant chain length favored the formation of layered and cubic phases. This stems from an increase of the surfactant packing factor  $g$ , i.e. the volume  $V$  increased more rapidly than the chain length  $l$ . Table 6 shows the XRD  $d_{100}$  spacings for as-synthesized MCM-41 type mesoporous  $\text{Nb}_2\text{O}_5$  (Nb-TMS1) samples prepared using a 0.5:1 surfactant to  $\text{Nb(OEt)}_5$  ratio and surfactant chain lengths of 12, 14, 16 and 18 carbon atoms. As seen, the wall thickness calculated as the difference between the unit cell parameter and the pore size diameter increased significantly with the surfactant chain length. A sample prepared with octadecylamine to  $\text{Nb(OEt)}_5$  ratio of 0.5 in the presence of 2 equiv. TMB was also included in Table 6. Addition of TMB increased the pore size up to a maximum of ca.  $39 \text{ \AA}$ . Contrary to MCM-41 silicates, further addition of swelling agent made little difference.

The same LAT strategy was also applied to the synthesis of mesoporous  $\text{Ta}_2\text{O}_5$  [138]. A hexagonal phase with pore size ranging from 20 to  $40 \text{ \AA}$  and a surface area of over  $500 \text{ m}^2 \text{ g}^{-1}$  was obtained. The material exhibited a butane adsorption capac-

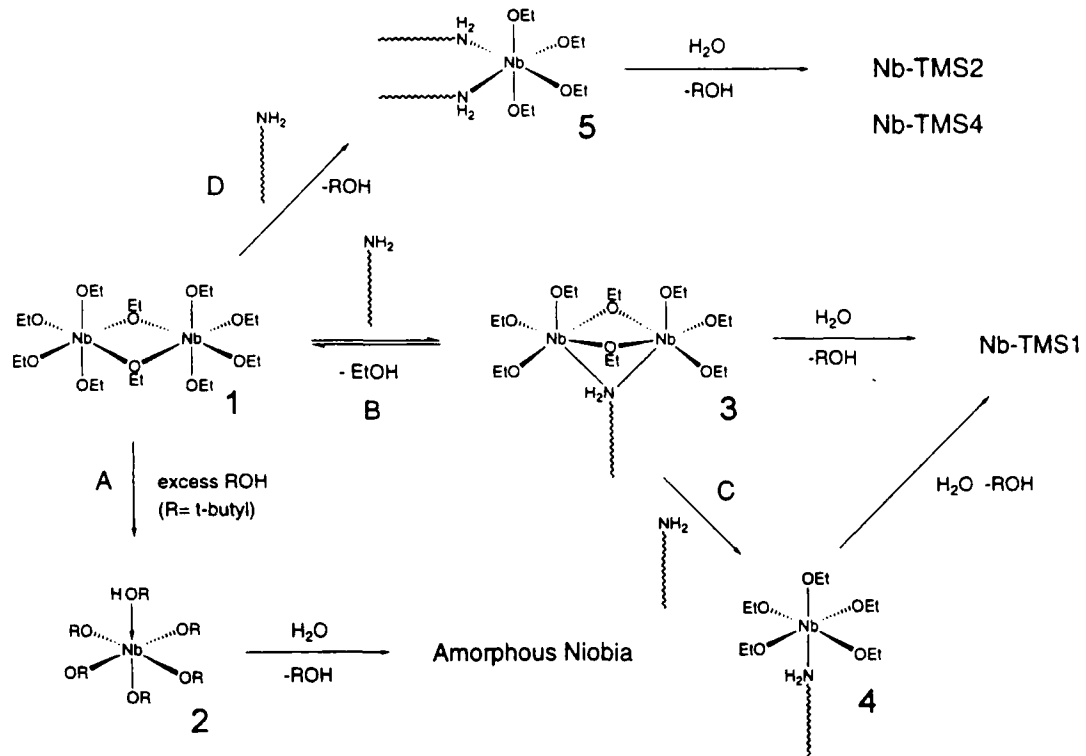


Fig. 18. Equilibrium in ethanol solution of  $\text{Nb}(\text{Oct})_5$  and amine surfactants showing the proposed pathways (A–D) of formation of Nb-TMS phases (Nb-TMS1: 2D hexagonal; Nb-TMS2: 3D hexagonal; and Nb-TMS4: layered structure) [139].

Table 6  
Variation of pore size of Nb-TMS1 with chain length and mesitylene [139]

Surfactant chain length	$d(100)$ ( $\text{\AA}$ )	Unit cell ( $\text{\AA}$ )	Pore size ( $\text{\AA}$ )	Wall thickness ( $\text{\AA}$ )
12	28	32.3	22	10.4
14	33	38.2	27	11.1
16	36	41.7	29	12.7
18	40	46.0	33	13.0
18 + 2 TMB	45	51.8	39	12.8

ity as high as  $95 \text{ cm}^3 \text{ g}^{-1}$  or  $0.28 \text{ g g}^{-1}$  at STP which compares favorably with the adsorption capacity of MCM-41 silicate.

As can be seen in Fig. 16, the success of the LAT approach depends largely on the selective hydrolysis of  $-\text{OEt}$  group followed by condensation between Nb (or Ta) species, while the Nb–N (or Ta–N) bond must be strong enough to resist the hydrolysis. The occurrence of a covalent bond may need further experimental support. Based on the available NMR data, the possibility of a tem-

plating mechanism via hydrogen bond formation cannot be dismissed, despite the fact that the surfactant in the resulting phase cannot be removed by simple extraction with alcohols in the absence of an acid.

#### 4.4. Mg- and Zn-based mesolamellar structures: yet another approach

Zhao and Goldfarb [143] used non-amphiphilic mesogens as templates to prepare Mg- and

Zn-based lamellar mesostructures at room temperature. Two non-amphiphilic molecules capable of forming lyotropic liquid crystals were used, namely disodium chromoglycate (DSCG) and flufenamic acid (FA). XRD and TEM data provided evidence that all samples were lamellar in nature. Furthermore, based on TGA,  $^{13}\text{C}$  NMR and IR data together with energy minimization calculations, it was proposed that the materials were comprised of inorganic layers separated by organic bilayers. The reduced IR frequencies of the carbonyl groups of the occluded organic molecules were considered as evidence that, in both cases, interfacial interactions between the organic and inorganic species involve the carboxylate groups. In addition, within the organic DSCG bilayer, there are additional interactions between the two layers via hydrogen bonding involving the hydroxyl groups. Sodium ions, found in significant amounts in the final materials, were thought to be located at the organic–inorganic interface close to the carboxylates and, together with protons, play the role of charge balancing species.

## 5. Discussion

While the supramolecular templating method was originally developed for the synthesis of mesoporous silicates and aluminosilicates, it was quickly adapted to the preparation of a large number of non-silica-based materials. This is in contrast to the development of non-silica inorganic structures homologous to zeolites where several decades of research generated only a limited number of successful combinations such as metallophosphates. This is largely due to the structural differences between long-range periodic and amorphous mesoporous materials on the one hand, and crystalline microporous zeotypes on the other. Indeed, microporous zeolitic materials are highly crystalline and accommodate framework metallic cation only in a tetrahedral environment. Because of these stringent geometric and energetic constraints, non-silica microporous crystalline (mixed) oxides akin to zeolites have a limited range of composition. In contrast, NMR and other techniques provided strong evidence that the pore walls of mesoporous

materials are amorphous, thus allowing for wide variations in bond angles, lengths and numbers as well as in local symmetry. The absence of specific local constraints in mesoporous molecular sieves allows the preparation of materials with much wider compositional diversity. The supramolecular templating method thus opens new horizons for the design of porous materials. In addition, as a result of extensive work on synthesis methods, new strategies such as templating via hydrogen or covalent bonding have been developed. However, as will be discussed hereafter, the synthesis of non-silica-based materials provides new challenges.

The search for non-silica mesoporous metal oxides using methods based on electrostatic interactions met limited success. First, most of the phases obtained were lamellar and consequently not resistant to thermal treatment. Second, even the three-dimensional structures (Pb, Sb and W oxides) did not withstand calcination or any other surfactant removal technique [35]. One possible reason for the lack of stability is that the inorganic part may not be well polymerized. For example, in the synthesis of  $\text{ZrO}_2$ , a highly acidic medium was often used, possibly preventing the polymerization of zirconium species into a strong enough structure [102]. As no careful investigations like those performed on Keggin ions of W and Nb–W were undertaken on most of the systems prepared via electrostatic interactions, the presence of unconnected inorganic species may actually be widespread. In some instances, the material may be stabilized by post-synthesis treatment [101,104]. The rich redox chemistry of some metal oxides may also be at the origin of their lack of thermal stability [35,96].

While searching for alternative methods, much attention was focused on the use of organometallic chemistry and organic solvents. Work on mesoporous titanium oxide [91] showed that interaction between the template and the inorganic species must be established before allowing the metal oxide to condense further. This was achieved by using acetylacetone as ligands, the presence of which slows down the rate of hydrolysis. The hydrolysis rate may also be decreased by using organic solvents and controlling the amount of

water. This was illustrated by Vaudry et al. [135] in the preparation of mesoporous alumina.

Though it was mentioned in earlier investigations that the neutral templating approach could be used for the preparation of mesoporous metal oxides, the only report available so far dealt with alumina [131]. This method is supposed to be convenient since the template can be removed by room temperature extraction with organic solvents. As a result, it may be an efficient method for the preparation of other metal oxides.

Up to now, in terms of pore structure periodicity, the best quality mesoporous metal oxides were produced by the LAT method. However, the covalent bonding is still limited to metal–nitrogen systems, thus preventing its wider application. The following is a non-exhaustive list of LAT related issues that are worth investigating in order to encourage future development of similar routes using other types of surfactant and organometallic precursor: (i) more definitive evidence of the proposed mechanism, particularly the occurrence of Me–N covalent bonding is desirable; (ii) so far only transition metal ethoxides were used as precursors, extension to other alkoxides, which are sometimes cheaper, should be pursued; (iii) LAT methods involving covalent bonding to atoms such as oxygen and sulfur should be developed.

So far, the FSM-16 surfactant intercalation approach afforded good quality mesoporous silicate [63,64] and vanadophosphate [95]. This effort is worth pursuing because this method may potentially lead to new mesoporous molecular sieves provided that suitable layered starting materials are available.

The success of obtaining a specific mesoporous metal oxide depends on two conditions, i.e. the occurrence of a three-dimensional mesophase and the stability of the inorganic shell upon removal of the surfactant. The structure of the material is to a first degree determined by the surfactant packing parameter,  $g$ . However, one must be careful in using the  $g$  factor to explain or predict the morphology of a mesophase. The head group area can sometimes be a vague concept. It was originally defined as the area of the head group of the surfactant in water. However, after the organic–inorganic interaction is established, the head group

should include the inorganic part. That was the reasoning used in the interpretation of the neutral templating mechanism. The large head group formed after connecting the inorganic species to the amine group via hydrogen bonding is consistent with the exclusive formation of hexagonal phases [53]. Likewise, the effective volume and length of the surfactant hydrophobic chain depend on the synthesis conditions, particularly the presence of co-solvents and expander molecules.

The stability of a mesophase is a more complicated issue. It certainly depends on the redox chemistry of the metal oxide. Equally important is the extent of condensation of the inorganic walls. A higher degree of polymerization imparts improved stability. The solution chemistry and redox properties of metallic species involved in the synthesis should be examined carefully. The polymerization of inorganic species is usually achieved by adjusting the pH or by hydrothermal treatment. Furthermore, the interaction between the surfactant and the inorganic wall should not be too strong, so that the surfactant can easily be removed. For this purpose, hydrogen bonding is more convenient than electrostatic interactions. The preparation of  $\text{Nb}_2\text{O}_5$  corresponds to a compromise situation. On the one hand, the Nb–N bond is strong enough to resist the hydrolysis and allow the condensation of Nb–O–Nb, and on the other hand, it is not too strong so that the amine surfactant can be removed by extraction with an alcoholic acid solution.

For syntheses involving organometallic precursors, the use of organic solvents in the presence of stoichiometric amounts of water is an effective method to decrease the hydrolysis rate. Also worth mentioning is that some surfactants such as alkyl carboxylic acids which are not soluble in water can now be used for the design of mesoporous oxides, thus providing additional flexibility.

Another issue with scientific merit is the crystallinity of the inorganic walls of mesoporous molecular sieves. So far, these walls have been almost exclusively amorphous. This may have some drawbacks compared to crystalline zeolitic materials. Examples include (i) low acidity of mesoporous aluminosilicates, (ii) poorly defined sites in transition metal modified silicates, and (iii) easy leach-

ing of metallic cations, e.g. easy dealumination [33] and deboronation [141,142]. Zirconium oxide was the first example of mesoporous materials with partially crystalline walls [111]. Mesoporous manganese oxide molecular sieves were also shown to be comprised of microcrystallites of dense phases of  $Mn_2O_3$  and  $Mn_3O_4$ . Additional crystalline mesoporous materials may be discovered in the near future.

Despite the increasing number of successful syntheses of non-silica mesostructured materials, little has been done to explore their potential applications. As far as catalytic properties are concerned, some data regarding gas phase acid catalysis over mesoporous zirconium oxide [35,110,111] and liquid phase oxidation catalysis over manganese oxide [113] are now available. However, the materials described here, and similar materials yet to be discovered, offer great opportunities for innovative applications not only in catalysis but also in advanced materials devices.

## 6. Concluding remarks

The current enthusiasm in the area of non-silica mesoporous materials is focused on the synthesis of metal oxides. The list of successful syntheses includes Nb, Al, Zr, Hf, Ta, Zr–P and Ti–P oxides. It was also mentioned that Ti, Ce and Y oxides may be prepared via the LAT technique, but no data have been reported so far. Three-dimensional mesostructured oxides of W, Pb, Sn, V and V–P have also been synthesized but were found to be unstable after removal of the surfactant. It remains a major challenge to stabilize their structure or to discover new or improved pathways to stable mesoporous molecular sieves. Additional efforts should aim at developing potential applications for non-silica mesostructured materials. As transition metal oxides have variable oxidation states, they may find applications involving their catalytic, electric and magnetic properties.

## Acknowledgement

The authors thank Dr. I.L. Moudrakovski, Dr. J. Liu, Dr. J.S. Reddy, Mrs. V.R. Karra, Dr. A.

Chenite, Dr. K.F. Preston, Dr. J.A. Ripmeester, Dr. C.I. Ratcliffe and Dr. Y. Le Page for their invaluable contributions.

## References

- [1] T.J. Pinnavaia, M.F. Thorpe (Eds.), *Access in Nanoporous Materials*, Plenum Press, New York, 1995.
- [2] S. Komereni, D.M. Smith, J.S. Beck (Eds.), *Advances in Porous Materials*, Materials Research Society, Pittsburgh, 1995.
- [3] T.J. Pinnavaia, H. Kim, in: E.G. Derouane et al. (Eds.), *Zeolite Microporous Solids: Synthesis, Structure, and Reactivity*, NATO ASI Series C, Vol. 352, Kluwer Academic, Dordrecht, 1992, p. 79.
- [4] H.C. Foley, M.S. Cane, J.F. Goellner, in: T.J. Pinnavaia, M.F. Thorpe (Eds.), *Access in Nanoporous Materials*, Plenum Press, New York, 1995, p. 39.
- [5] C.J. Brinker, G.W. Scherer, *Sol-Gel Science, The Physics and Chemistry of Sol-Gel Processing*, Academic Press, San Diego, 1990.
- [6] F. Cando, in: *Encyclopedia of Polymer Science Engineering*, Vol. 9, Wiley, New York, 1987, p. 718.
- [7] M.A. El-Nokaly (Ed.), *Polymer Association Structures: Microemulsions and Liquid Crystals*, ACS Symp. Ser. No. 384, ACS, Washington, DC, 1989.
- [8] C.G. Coe, in: T.J. Pinnavaia, M.F. Thorpe (Eds.), *Access in Nanoporous Materials*, Plenum Press, New York, 1995, p. 213.
- [9] A. Dyer, *An Introduction to Zeolite Molecular Sieves*, Chapter 7, Wiley, Chichester, 1988.
- [10] M. Suzuki, *Adsorption Engineering*, Elsevier, Amsterdam, 1990.
- [11] R.P. Towsend, *Stud. Surf. Sci. Catal.* 58 (1991) 571.
- [12] S.T. Sie, *Stud. Surf. Sci. Catal.* 85 (1994) 587.
- [13] W.F. Hölderich, H. van Bekkum, *Stud. Surf. Sci. Catal.* 58 (1991) 631.
- [14] M.E. Davis, *Ind. Eng. Chem. Res.* 30 (1991) 1675.
- [15] G.A. Ozin, A. Kuperman, A. Stein, *Angew. Chem. Int. Ed.* 28 (1989) 359.
- [16] V.I. Srdanov, N.P. Blake, D. Markgraber, H. Metiu, G.D. Stucky, *Stud. Surf. Sci. Catal.* 85 (1994) 115 and references cited therein
- [17] G. Schulz-Ekloff, *Stud. Surf. Sci. Catal.* 85 (1994) 145.
- [18] P. Behrens, G.D. Stucky, *Angew. Chem. Int. Ed. Engl.* 32 (1993) 696.
- [19] J.F. Joly, A. Merrouche, H. Kessler, J.L. Guth, Fr. Patent No. 91 03378 (1991).
- [20] M.E. Davis, C. Saldarriaga, C. Montes, J.M. Garces, C.A. Crowder, *Nature* 331 (1988) 698.
- [21] M. Estermann, L.B. McCusker, Ch. Baerlocher, A. Merrouche, H. Kessler, *Nature* 352 (1991) 320.
- [22] Q. Huo, R. Xu, S. Li, Z. Ma, J.M. Thomas, R.H. Jones, A.M. Chippindale, *J. Chem. Soc., Chem. Commun.* (1992) 875.

- [23] T. Loiseau, G. Ferrey, *J. Solid State Chem.* 111 (1994) 403.
- [24] C.C. Freyhardt, M. Tsapatsis, R.F. Lobo, K.J. Balkus, M.E. Davis, *Nature* 381 (1996) 295.
- [25] H. van Bekkum, E.M. Flanigen, J.C. Jansen (Eds.), *Introduction to Zeolite Science and Practice*, Stud. Surf. Sci. Catal. No. 58, Elsevier, Amsterdam, 1991.
- [26] J.C. Jansen, M. Stöcker, H.G. Karge, J. Weitkamp (Eds.), *Advanced Zeolite Science and Applications*, Stud. Surf. Sci. Catal. No. 85, Elsevier, Amsterdam, 1994.
- [27] H. Chon, S.I. Woo, S.E. Park (Eds.), *Recent Advances and New Horizons in Zeolite Science and Technology*, Stud. Surf. Sci. Catal. No. 102, Elsevier, Amsterdam, 1996.
- [28] R. Szostak, *Molecular Sieves: Principles of Synthesis and Identification*, Van Nostrand Reinhold, New York, 1989.
- [29] P.A. Jacobs, J.A. Martens, *Synthesis of Aluminosilicate Zeolites*, Stud. Surf. Sci. Catal. No. 33, Elsevier, Amsterdam, 1987.
- [30] C.T. Kresge, M.E. Leonowicz, W.J. Roth, J.C. Vartuli, J.S. Beck, *Nature* 359 (1992) 710.
- [31] J.S. Beck, J.C. Vartuli, W.J. Roth, M.E. Leonowicz, C.T. Kresge, K.D. Schmitt, C.T.-W. Chu, D.H. Olson, E.W. Sheppard, S.B. McCullen, J.B. Higgins, J.L. Schlenker, *J. Am. Chem. Soc.* 114 (1992) 10834.
- [32] A. Sayari, *Chem. Mater.* 8 (1996) 1840.
- [33] A. Sayari, *Stud. Surf. Sci. Catal.* 102 (1996) 1.
- [34] X. Zhao, G.Q. Liu, G.J. Millar, *Ind. Eng. Chem. Res.* 35 (1996) 2075.
- [35] F. Schüth, *Ber. Bunsenges. Phys. Chem.* 99 (1995) 1306.
- [36] N.K. Raman, M.T. Anderson, C.J. Brinker, *Chem. Mater.* 8 (1996) 1682.
- [37] G.D. Stucky, Q. Huo, A. Firouzi, B.F. Chmelka, S. Schacht, I.G. Voigt-Martin, F. Schüth, *Stud. Surf. Sci. Catal.* 105 (1996) 3.
- [38] J. Liu, A.Y. Kim, L.Q. Wang, B.J. Palmer, Y.L. Chen, P. Bruinsma, B.C. Bunker, G.J. Exharhos, G.L. Graff, P.C. Rieke, G.E. Fryxell, J.W. Virden, B.J. Tarasevich, L.A. Chick, *Adv. Colloid Interface Sci.* 69 (1996) 131.
- [39] Q. Huo, D.I. Margolese, U. Ciesla, P. Feng, T.E. Gier, P. Sieger, R. Leon, P.M. Petroff, F. Schüth, G.D. Stucky, *Nature* 368 (1994) 317.
- [40] Q. Huo, D.I. Margolese, U. Ciesla, D.G. Demuth, P. Feng, T.E. Gier, P. Sieger, A. Firouzi, B.F. Chmelka, F. Schüth, G.D. Stucky, *Chem. Mater.* 6 (1994) 1176.
- [41] U. Ciesla, D. Demuth, R. Leon, P.M. Petroff, G. Stucky, K. Unger, F. Schüth, *J. Chem. Soc., Chem. Commun.* (1994) 1387.
- [42] J.C. Vartuli, C.T. Kresge, M.E. Leonowicz, A.S. Chu, S.B. McCullen, I.D. Johnson, E.W. Sheppard, *Chem. Mater.* 6 (1994) 2070.
- [43] J.S. Beck, J.C. Vartuli, G.J. Kennedy, C.T. Kresge, W.J. Roth, S.E. Schramm, *Chem. Mater.* 6 (1994) 1816.
- [44] J.C. Vartuli, K.D. Schmitt, C.T. Kresge, W.J. Roth, M.E. Leonowicz, S.B. McCullen, S.D. Hellring, J.S. Beck, J.L. Schlenker, D.H. Olson, E.W. Sheppard, *Chem. Mater.* 6 (1994) 2317; *Stud. Surf. Sci. Catal.* 84 (1994) 53.
- [45] C.F. Cheng, Z. Luan, J. Klinowski, *Langmuir* 11 (1995) 2815.
- [46] A. Monnier, F. Schüth, Q. Huo, D. Kumar, D. Margolese, R.S. Maxwell, G.D. Stucky, M. Krishnamurti, P. Petroff, A. Firouzi, M. Janicke, B.F. Chmelka, *Science* 261 (1993) 1299.
- [47] G.D. Stucky, A. Monnier, F. Schüth, Q. Huo, D. Margolese, D. Kumar, M. Krishnamurti, P. Petroff, A. Firouzi, M. Janicke, B.F. Chmelka, *Mol. Cryst. Liq. Cryst.* 240 (1994) 187.
- [48] A. Firouzi, A. Monnier, L.M. Bull, T. Besier, P. Sieger, Q. Huo, S.A. Walker, J.A. Zasadzinski, C. Glinka, J. Nicol, D. Margolese, G.D. Stucky, B.F. Chmelka, *Science* 267 (1995) 1138.
- [49] L.M. Bull, D. Kumar, S.P. Millar, T. Besier, M. Janicke, G.D. Stucky, B.F. Chmelka, *Stud. Surf. Sci. Catal.* 84 (1994) 429.
- [50] C.J. Glinka, J.M. Nicol, G.D. Stucky, E. Ramli, D.I. Margolese, Q. Huo, *Mater. Res. Soc. Symp. Proc.* 371 (1995) 47.
- [51] A. Firouzi, F. Atef, A.G. Oertli, G.D. Stucky, B. Chmelka, *J. Am. Chem. Soc.* 119 (1997) 3596.
- [52] P.T. Tanev, T.J. Pinnavaia, *Science* 267 (1995) 865.
- [53] P.T. Tanev, T.J. Pinnavaia, in: T.J. Pinnavaia, M.F. Thorpe (Eds.), *Access in Nanoporous Materials*, Plenum Press, New York, 1995, p. 13.
- [54] P.T. Tanev, T.J. Pinnavaia, *Mater. Res. Soc. Symp. Proc.* 371 (1996) 63.
- [55] S.A. Bagshaw, E. Prouzet, T.J. Pinnavaia, *Science* 269 (1995) 1242.
- [56] P.T. Tanev, J.T. Pinnavaia, *Chem. Mater.* 8 (1996) 2068.
- [57] J.N. Israelachvili, *Intermolecular and Surface Forces*, Chapter 17, Academic Press, London, 1992.
- [58] J.N. Israelachvili, D.J. Mitchell, B.W. Ninham, *J. Chem. Soc., Faraday Trans. II* 76 (1976) 1527.
- [59] Q. Huo, D.I. Margolese, G.D. Stucky, *Chem. Mater.* 8 (1996) 1147.
- [60] G.S. Attard, J.C. Glyde, C.G. Göltner, *Nature* 378 (1995) 366.
- [61] T. Yanagisawa, T. Shimizu, K. Kuroda, C. Kato, *Bull. Chem. Soc. Jpn.* 63 (1990) 988.
- [62] S. Inagaki, Y. Fukushima, K. Kuroda, *J. Chem. Soc., Chem. Commun.* (1993) 680.
- [63] S. Inagaki, A. Koizumi, N. Suzuki, Y. Fukushima, K. Kuroda, *Bull. Chem. Soc. Jpn.* 69 (1996) 1449 and references cited therein.
- [64] C.Y. Chen, S.Q. Xiao, M.E. Davis, *Microporous Mater.* 4 (1995) 1.
- [65] S. Oliver, A. Kuperman, N. Coombs, A. Lough, G.A. Ozin, *Nature* 378 (1995) 47.
- [66] A. Chenite, Y. Le Page, V.R. Karra, A. Sayari, *J. Chem. Soc., Chem. Commun.* (1996) 413.
- [67] P.T. Tanev, T.J. Pinnavaia, *Science* 271 (1996) 1267.
- [68] Q. Huo, R. Leon, P.M. Petroff, G.D. Stucky, *Science* 268 (1995) 1324.
- [69] M. Clerc, *J. Phys. II, Fr.* 6 (1996) 961.
- [70] M. Kruk, M. Jaroniec, A. Sayari, *J. Phys. Chem. B* 101 (1997) 583 and references cited therein

- [71] N. Ulagappan, C.N.R. Rao, *Chem. Commun.* (1996) 2759.
- [72] D. Khushalani, A. Kuperman, G.A. Ozin, K. Tanaka, J. Garces, M.M. Olken, N. Coombs, *Adv. Mater.* 7 (1995) 842.
- [73] A. Sayari, P. Liu, M. Kruk, M. Jaroniec, *Chem. Mater.* (1997) in press.
- [74] M.T. Anderson, J.E. Martin, J. Odinek, P. Newcomer, in: T.J. Pinnavaia, M.F. Thorpe (Eds.), *Access in Nanoporous Materials*, Plenum Press, New York, 1995, p. 29.
- [75] D. Khushalani, A. Kuperman, N. Coombs, G.A. Ozin, *Chem. Mater.* 8 (1996) 2188.
- [76] C.F. Cheng, W. Zhou, D.H. Park, J. Klinowski, M. Hargreaves, L.F. Gladden, *J. Chem. Soc., Faraday Trans.* 93 (1997) 359.
- [77] C.N. Wu, T.S. Tsai, C.N. Liao, K.J. Chao, *Microporous Mater.* 4 (1996) 173.
- [78] J.S. Reddy, A. Dicko, A. Sayari, in: *Synthesis of Porous Materials: Zeolites, Clays, Nanostructures*, M.L. Occelli, H. Kessler, Eds., Marcel Dekker, 1996, p. 405.
- [79] A. Sayari, I.L. Moudrakovski, C.I. Ratcliffe, J.A. Ripmeester, K.F. Preston, in: M.L. Occelli, H. Kessler (Eds.), *Synthesis of Porous Materials: Zeolites, Clays and Nanostructures*, Marcel Dekker, New York, 1996, p. 417.
- [80] M.E. Davis, C.Y. Chen, S.L. Burkett, R.F. Laubo, *Mater. Res. Soc. Symp. Proc.* 346 (1994) 831.
- [81] R. Schmidt, M. Stöcker, O.H. Ellestad, *Stud. Surf. Sci. Catal.* 97 (1995) 149.
- [82] A. Steel, S.W. Carr, M.W. Anderson, *Chem. Mater.* 7 (1995) 1829.
- [83] C.Y. Chen, H.X. Li, M.E. Davis, *Microporous Mater.* 2 (1993) 17.
- [84] M. Fröba, P. Behrens, J. Wong, G. Engelhardt, Ch. Haggemüller, G. van de Goor, M. Rowen, T. Tanaka, W. Schweiher, *Mater. Res. Soc. Symp. Proc.* 371 (1995) 99.
- [85] A. Liepold, K. Roos, W. Roschetilowski, A.P. Esculas, J. Rocha, A. Philippou, M.W. Anderson, *J. Chem. Soc., Faraday Trans.* 92 (1996) 4623.
- [86] A. Stein, M. Fendorf, T.P. Jarvie, K.T. Mueller, A.J. Benesi, T.E. Mallouk, *Chem. Mater.* 7 (1995) 304.
- [87] A. Stein, M. Fendorf, T.P. Jarvie, K.T. Mueller, M.E. Garcia, T.E. Mallouk, *Mater. Res. Soc. Symp. Proc.* 371 (1995) 69.
- [88] G.G. Janauer, A. Dobley, J. Guo, P. Zavalij, M.S. Whittingham, *Chem. Mater.* 8 (1996) 2096.
- [89] S.B. McCullen, J.C. Vartuli, US Patent No. 5 156 829 (1992).
- [90] N. Ulagappan, C.N.R. Rao, *Chem. Commun.* (1996) 1685.
- [91] D.M. Antonelli, J.Y. Ying, *Angew. Chem. Int. Ed. Engl.* 34 (1995) 2014.
- [92] V. Luca, D.J. MacLachlan, J.M. Hook, R. Withers, *Chem. Mater.* 7 (1995) 2220.
- [93] G.G. Janauer, A.D. Dobley, P.Y. Zavalij, M.S. Whittingham, *Chem. Mater.* 9 (1997) 647.
- [94] T. Abe, A. Taguchi, M. Iwamoto, *Chem. Mater.* 7 (1995) 1429.
- [95] T. Doi, T. Miyake, *Chem. Commun.* (1996) 1635.
- [96] P. Liu, I.L. Moudrakovski, J. Liu, A. Sayari, *Chem. Mater.* (1997) in press.
- [97] H.P. Lin, C.Y. Mou, *Science* 273 (1996) 765.
- [98] S. Schacht, Q. Huo, I.G. Voigt-Martin, G.D. Stucky, F. Schüth, *Science* 273 (1996) 768.
- [99] Y. Yang, N. Coombs, G.A. Ozin, *Nature* 386 (1997) 692.
- [100] X. Song, A. Sayari, *Catal. Rev.-Sci. Eng.* 38 (1996) 329.
- [101] A. Sayari, P. Liu, J.S. Reddy, *Mater. Res. Soc. Symp. Proc.* 431 (1996) 101.
- [102] J.S. Reddy, A. Sayari, *Catal. Lett.* 38 (1996) 219.
- [103] P. Liu, J. Liu, A. Sayari, unpublished data.
- [104] U. Ciesla, S. Schacht, G.D. Stucky, K.K. Unger, F. Schüth, *Angew. Chem. Int. Ed. Engl.* 35 (1996) 541.
- [105] J.A. Knowles, M.J. Hudson, *J. Chem. Soc., Chem. Commun.* (1995) 2083.
- [106] J.A. Knowles, M.J. Hudson, *J. Mater. Chem.* 6 (1996) 89.
- [107] A.Y. Kim, P.J. Bruinsma, Y.L. Chen, J. Liu, *Mater. Res. Soc. Symp. Proc.* 435 (1996) 131.
- [108] A.Y. Kim, P.J. Bruinsma, Y.L. Chen, L.Q. Wang, J. Liu, *Chem. Commun.* (1997) 161.
- [109] G. Pacheco, E. Zhao, A. Garcia, A. Sklyarov, J.J. Fripiat, *Chem. Commun.* (1997) 491.
- [110] G. Larsen, E. Lotero, M. Nabity, L.M. Petkovic, D.S. Shobe, *J. Catal.* 164 (1996) 246.
- [111] Y.Y. Huang, T.J. McCarthy, W.M.H. Sachtler, *Appl. Catal.* 148 (1996) 135.
- [112] P. Liu, J. Liu, A. Sayari, *Chem. Commun.* (1997) 577.
- [113] Z.R. Tian, W. Tong, J.Y. Wang, N.G. Duan, V.V. Krishnan, S.L. Suib, *Science* 276 (1997) 926.
- [114] S.L. Suib, *Stud. Surf. Sci. Catal.* 102 (1996) 47 and related references therein.
- [115] M.T. Anderson, P. Newcomer, *Mater. Res. Soc. Symp. Proc.* 371 (1995) 117.
- [116] P.V. Braun, P. Osenar, S.I. Stupp, *Nature* 380 (1996) 325.
- [117] J. Li, L. Delmotte, H. Kessler, *Chem. Commun.* (1996) 1023.
- [118] J. Li, H. Kessler, L. Delmotte, *J. Chem. Soc., Faraday Trans.* 93 (1997) 665.
- [119] A. Sayari, I.L. Moudrakovski, J.S. Reddy, C.I. Ratcliffe, J.A. Ripmeester, K.F. Preston, *Chem. Mater.* 8 (1996) 2080.
- [120] C.A. Fyfe, W. Schweiher, G. Fu, G.T. Kokotailo, H. Grondey, *Preprints Div. Petrol. Chem.* 40 (1995) 266.
- [121] G.A. Ozin, S. Oliver, *Adv. Mater.* 7 (1995) 943.
- [122] S. Oliver, N. Coombs, G.A. Ozin, *Adv. Mater.* 7 (1995) 931.
- [123] G.A. Ozin, *Acc. Chem. Res.* 30 (1997) 17.
- [124] Q. Gao, J. Chen, R. Xu, Y. Yue, *Chem. Mater.* 9 (1997) 457.
- [125] A. Sayari, V.R. Karra, J.S. Reddy, I.L. Moudrakovski, *J. Chem. Soc., Chem. Commun.* (1996) 411.
- [126] A. Sayari, *Stud. Surf. Sci. Catal.* 105 (1996) 37.
- [127] T. Kimura, Y. Sugahara, K. Kuroda, in: *Book of*

- Abstracts, 11th International Zeolite Conference, Seoul, Korea, 1996, Paper RP45.
- [128] P. Feng, Y. Xia, J. Feng, X. Bui, G.D. Stucky, *Chem. Commun.* (1997) 949.
- [129] B. Chakraborty, A.C. Pulikottil, S. Das, B. Viswanathan, *Chem. Commun.* (1997) 911.
- [130] S. Ayyappan, C.N.R. Rao, *Chem. Commun.* (1997) 575.
- [131] S.A. Bagshaw, T.J. Pinnavaia, *Angew. Chem. Int. Ed. Engl.* 35 (1996) 1102.
- [132] E.P. Barrett, L.G. Joyner, P.P. Halender, *J. Am. Chem. Soc.* 73 (1951) 373.
- [133] J.W. Akitt, *Prog. Nucl. Magn. Reson. Spectrosc.* 21 (1989) 127.
- [134] M. Yada, M. Machinda, T. Kijima, *Chem. Commun.*, (1996) 769.
- [135] F. Vaudry, S. Khodabandeh, M.E. Davis, *Chem. Mater.* 8 (1996) 1451.
- [136] M. Kruk, M. Jaroniec, A. Sayari, *Microporous Mater.* 9 (1997) 173.
- [137] D.M. Antonelli, J.Y. Ying, *Angew. Chem. Int. Ed. Engl.* 35 (1996) 426.
- [138] D.M. Antonelli, J.Y. Ying, *Chem. Mater.* 8 (1996) 874.
- [139] D.M. Antonelli, A. Nakahira, J.Y. Ying, *Inorg. Chem.* 35 (1996) 3126.
- [140] D.M. Antonelli, J.Y. Ying, *Curr. Op. Colloid Interface Sci.* 1 (1996) 523.
- [141] U. Oberhagemann, I. Kinski, I. Dierdorf, B. Marler, H. Gies, *J. Non-Cryst. Mater.* 197 (1996) 145.
- [142] A. Sayari, I. Moudrakovski, C. Danumah, C.I. Ratcliffe, J.A. Ripmeester, K.F. Preston, *J. Phys. Chem.* 99 (1995) 16373.
- [143] D. Zhao, D. Goldfarb, *Chem. Mater.* 8 (1996) 2571.